A PROPOSAL TO MEASURE DIRECT PHOTON PRODUCTION AT TEVATRON ENERGIES

W. Baker, J. Biel, T. Droege, D. Eartly, A. Jonckheere, P. Koehler,
A. Lennox and C. A. Nelson, Jr.
Fermilab
C. Bromberg, S. Cooper, R. A. Lewis, R. Miller, B. Y. Oh,
G. A. Smith and J. Whitmore
Michigan State University
K. Heller, M. Marshak, E. Peterson, J. Povlis, K. Ruddick and M. Shupe
University of Minnesota
D. Garelick. G. Glass, M. Glaubman, S. Hossain, E. Pothier
and Han Shu-Rong
Northeastern University
W. E. Cleland, E. Engels, Jr., P. F. Shepard and J. A. Thompson
University of Pittsburgh
S. Cihangir, T. Ferbel, J. Huston, F. Lobkowicz, M. McLaughlin, S. Olsen,
P. Slattery and M. Zielinski
University of Rochester

Correspondents:

P. Slattery
University of Rochester
Rochester, N.Y. 14627
(716) 275-4368

C. A. Nelson, Jr.
Fermilab
Batavia, IL. 60510
(312) 840-4294

Submitted:

October 26, 1981

ABSTRACT

We propose to examine the production of direct photons at large transverse momenta in hadron-nucleon collisions at Tevatron energies. We intend to construct a new large-acceptance spectrometer that will enable us to measure with precision the properties of events that contain one or more photons with $p_T \gtrsim 5$ GeV/c. The primary goal of this experiment is to obtain information on quark and gluon interactions through studying the yield of single direct photons and their accompanying hadrons in collisions of π^+, π^- and p with nucleons. In particular, we will determine the gluon structure functions of the pion and the nucleon from rates extracted for the fundamental reactions $qg \to q\gamma$ (Compton process) and $\bar{q}q \to g\gamma$ (Annihilation process); we will also measure the fragmentation properties of the gluons and quarks that accompany photons in these reactions. We expect, in addition, to extract the signal for the simultaneous production of two primary photons in order to gain information on the $\bar{q}q \to \gamma\gamma$ process. This elementary reaction, expected to occur at approximately the level of $\bar{q}q \to \ell^+\ell^-$, offers in parallel with the Drell-Yan process, a particularly clean test of predictions from QCD. A unique feature of our proposed investigation is that we will be able to carry out a direct comparison of these two fundamental processes by comparing our $\gamma\gamma$ and e^+e^- triggered events.

The experiment is to be performed using 400 GeV/c protons, 530 GeV/c $\pi^\pm$ and protons, and 800 GeV/c protons, with beam intensities $\gtrsim 10^7$ per second. Assuming a 25% duty factor for the Tevatron, we require 2400 hours of beam time to complete our investigation; of this, 400 hours will be employed for setup and debugging of the apparatus.

I. PHYSICS MOTIVATION

The fundamental nature and underlying importance of direct photon production at large values of transverse momentum would appear to be sufficiently well-established at this time that an extended discussion in each new experimental proposal is no longer appropriate.[1] Indeed, the recent approval at CERN of four such experiments[2] is a rather unambiguous indication of just how great an importance is currently assigned to this type of investigation within the overall high energy physics community. These approvals are all the more noteworthy considering the enormous improvement which can be achieved in such experiments at Tevatron energies (see below).

Briefly summarized, the fundamental importance of the study of direct photon production arises from the elementary nature of the photon and its well-understood electromagnetic coupling. Any hard scattering process that has a gluon emitted from a quark vertex can also provide a photon, albeit with a cross section reduced by the ratio of the electromagnetic and strong coupling constants. By virtue of their elementary nature, such directly-produced photons can emerge as free particles, carrying all the p_T that was imparted to them in the primary collision, whereas the gluons, in contrast, must fragment into hadrons of reduced p_T. Not only does this significantly different behavior serve to enhance the γ/π^0 ratio at large p_T, and indeed this ratio is expected to approach unity at the transverse momentum values which we propose to study in this experiment, but even more significantly, and in marked contrast to the situation which prevails in experiments that rely on triggers involving high p_T hadrons, it is not necessary with high-p_T photons to unfold an additional fragmentation process before getting at the fundamental underlying quark and gluon dynamics.

At large p_T, direct photons are expected to originate mainly from two kinds of hard scattering processes. In p-nucleon and π^+-nucleon collisions

the Compton reaction $qg \rightarrow q\gamma$ should dominate, while in π^--nucleon collisions, even at moderate values of x_T (0.3 to 0.6), the annihilation reaction $\bar{q}q \rightarrow g\gamma$ should be just as important.[3] Several of the graphs of interest are illustrated in Fig. 1. The contribution from $gg \rightarrow g\gamma$, through a four-quark loop, has been estimated to be negligible.[4] We see that whenever a photon appears in the final state, it must either be accompanied by a gluon, in which case we can study gluon fragmentation, or the scattering had to be initiated by a gluon, in which case we can determine the gluon structure function of the incident hadron.

An important consequence of the C-invariance of the strong interactions is that the Compton graphs for π^+-nucleon and π^--nucleon collisions are the same, and therefore any difference in the yield of direct photons for these charge conjugate beams can be attributed to the annihilation graph. This point has been emphasized by R. Petronzio[5] and by R. Hagelberg et al[2], and a difference measurement has been proposed for determining the contribution of the annihilation diagram. We plan to take full advantage of this theoretical simplification in the course of our data analysis. (See also the discussion below of target material for further comments.)

The highest energy of the proton beam for this experiment was chosen to be the maximum expected for normal Tevatron operation. The energies for the pion beams were picked so as to have the same incident momentum per valence constituent as in the case of the proton; this may facilitate comparison of our data with theoretical models. In order to examine the question of the scaling of the cross section for direct-photon production, we will compare data obtained at 800 GeV/c with that at 400 GeV/c. In addition, we anticipate that, tagging protons and π^+ in the 530 GeV/c beam with the aid of a transition radiation detector system, we will also have an intermediary point for comparison.

The only reliable information on direct photon production thus far is from work with proton beams. The bulk of that data is from the ISR[6], where there is now evidence from two groups[7] that the topology of the events at large p_T is consistent with dominance of the Compton graph. Before employing an explicit model for p- and $\pi^{\pm}$-nucleon collisions at our proposed energies, we first provide an approximate indication of the level of improvement which we can expect to obtain relative to the experiments being presently mounted at the CERN SPS.

Figure 2 displays the energy dependence of the π^o yield measured in pp collisions for some representative p_T values; the curves have each been normalized to the yield at 200 GeV/c. The figure reflects the observed $(1-x_T)^9$ growth with energy of the π^o invariant cross section at fixed high p_T values. The relevance of these data in the present context arises from the observation made at the ISR that the γ/π^o ratio at fixed values of p_T is essentially independent of energy. Even though this result is somewhat inconsistent with expectations from simple QCD, it nevertheless provides a convenient phenomenological means for estimating direct photon yields in pp collisions. The figure indicates that, given an energy independent γ/π^o ratio, dramatic increases in direct photon yields at high p_T values are predicted between 200 GeV/c and Tevatron energies. For example, at p_T=6 GeV/c the predicted gain is more than 2 orders of magnitude, while at p_T=7 GeV/c, it is more than 3 orders of magnitude, between an experiment run at 800 GeV/c and one run at 200 GeV/c (such as E629).

For incident pions, the energy variation of the π^o yield, while expected to be qualitatively similar, need not, of course, be quantitatively identical. To obtain an estimate of what might be expected, we use the results of Fermilab experiment E258 for the reactions $\pi^- p \rightarrow \pi^{\pm} + \ldots$ at 200 and 300 GeV/c.[8] In this experiment both the π^+ and π^- yields are observed to vary

with energy at fixed p_T in proportion to $(1-x_T)^8$. Assuming this same variation for the π^o yield as well, we display in Fig. 3 the predicted growth of the π^o yield for $\pi^- p$ collisions between 200 GeV/c (the energy of the approved CERN SPS experiments) and 530 GeV/c (the energy of our proposed Tevatron experiment). Quantitatively, the improvement thus predicted is only slightly less dramatic than that measured in the pp case; a factor of $\sim$50 at p_T=6 GeV/c and of $\sim$250 at p_T=7 GeV/c. Viewed in an alternate way, and again assuming an energy independent γ/π^o ratio, at the Tevatron we can expect to observe as many direct photons at p_T^2=60 $(\text{GeV/c})^2$ as will be seen at p_T^2=35 $(\text{GeV/c})^2$ in the CERN SPS experiments. (This estimate does not have folded into it an additional anticipated rise of the γ/π^o ratio with increasing p_T; the acceptances of the various experiments are all comparable.) In our proposed experiment, we expect to sample direct photon production up to p_T^2 values of $\sim$100 $(\text{GeV/c})^2$. Because a factor of just 2 or 3 in Q^2, while nominally affecting α_s only slightly ($\sim$10%), can provide for a far cleaner test of QCD phenomenology,[9] this is, therefore, a significant improvement over even the most optimistic expectations for the lower energy experiments. Futhermore, the experiments which have recently been approved to run at the CERN SPS will lack the fine-grained, high resolution, photon detection capability that is so essential for an optimum experiment of this type.

In addition to investigating the dynamics of single photon production at high p_T, we also wish to extract the signal for the production of two direct photons. The two leading contributions are depicted in Fig. 4. The yield for this process is expected to be comparable to that for Drell-Yan annihilation into lepton pairs. In contrast to the case of single-γ production, the contribution of $gg \to \gamma\gamma$ may here be comparable to that from $\bar{q}q \to \gamma\gamma$.[10] Once again the π^+/π^- beam comparison can be used to extract the annihilation

diagram. Roughly speaking, the contribution of the annihilation process to the two γ cross section can be expected to be about $\alpha/\alpha_s \sim (1/137)/(1/4) \sim 1/35$ of the contribution of the reaction $\bar{q}q \to g\gamma$ to the single γ cross section. Consequently, exclusive of any contribution from the $gg \to \gamma\gamma$ diagram[11], the rate for the two photon process in π^--nucleon collisions can be expected to be approximately 1/70 of that for the production of a single γ. Taken literally, this would imply that an experiment which is designed to measure single photons up to p_T values of $\sim$10 GeV/c should also be able to investigate the two photon continuum up to masses of $\sim$16 GeV, corresponding to two photons with approximately equal, but opposing, values of $p_T \simeq 8$ GeV/c. (This estimate assumes a variation of the invariant cross section for single γ production with p_T in proportion to $(1-x_T)^8/p_T^8$, in agreement with the measured rate for $\pi^\pm$ production at 200 and 300 GeV/c; it is not intended to be more than a rough approximation to reality.)

Our interest in the two photon process stems not only from the fact that it can provide an important source of information concerning the gluon distribution in hadrons, but also because the process $\bar{q}q \to \gamma\gamma$ is a fundamental interaction, akin to the Drell-Yan process (see Fig. 4). If higher-order QCD corrections for the two reactions differ, then it is especially important to check whether the same discrepancy (by a factor of $\sim$2.4) between theory and experiment will be found in the $\gamma\gamma$ case as has been uncovered in the Drell-Yan case. This might provide a very significant test of the reliability of the perturbative QCD approach to the study of strong interactions.[12] We should add that the experimental trigger we expect to use for collecting data on 2-γ events will automatically provide us with a comparable sample of massive Drell-Yan e^+e^- pairs (as well as $\sim$100 $\Upsilon \to e^+e^-$ decays). We believe that such a direct comparison of $\gamma\gamma$ and e^+e^- yields in a single experiment should prove to be particularly illuminating.

The preceeding estimates are only intended to provide a rough guide to the overall sensitivity of our proposed experiment. More detailed, and more model dependent, estimates of yields will be presented below. We also wish to observe that we will of necessity also collect data containing multi-photon events. These data will permit us to search for possible high mass narrow states in relatively unexplored channels such as $\pi^o\gamma$, $\eta^o\gamma$, $\pi^o\eta^o$, $\eta^o\eta^o$, etc. Despite the potential for exciting surprises, we choose not to emphasize this aspect of the proposal in arguing for its approval.

Finally, it is appropriate to mention the kind of competition we can expect from the ISR and the CERN $\bar{p}p$ collider over the next several years. There is, of course, substantial overlap in the types of problems which can be challenged. In particular, gluon fragmentation and the annihilation process $\bar{q}q \rightarrow g\gamma$ can be studied very well with $\bar{p}p$ interactions. However, the anticipated relative loss of a factor of $\sim$20 in luminosity (even at the low-β regions of the colliders) and problems of geometry will make these experiments exceptionally difficult. We believe that our proposal will certainly be competitive with any such experiment that might be envisioned at the ISR. Interactions at the colliders (both CERN and Fermilab), although at comparable p_T, will be in a totally new domain, and we cannot judge their outcome. In any case, however, our data will be mainly at moderate values of x_T ($\sim$.4), while the data from the colliders will be primarily for $x_T \lesssim .04$. In this sense, the two sets of data will be complementary, and a comparison of relative photon yields, and of the nature of the accompanying hadrons, should prove to be quite informative.

II. EXPERIMENTAL ARRANGEMENT

A. Overview

Two major considerations have guided us in our design of the P695 apparatus: 1) Our conviction that the inherent difficulty of a direct-photon measurement required the availability of an exceptionally fine electromagnetic-shower detector, and 2) Our firm belief that a large-acceptance magnetic spectrometer was essential for a definitive investigation of the fragmentation properties of the constituents that are produced in association with the photons. The experience in the detection of photons that we gained as a result of the successful execution of experiment E629 (see Appendix A) has had major impact on the design features of the photon detector for P695. Our choice of elements for the rest of the apparatus has been based primarily on our Monte-Carlo investigations of the fragmentation of constituents, using the Feynman-Field parameterization.[13]

Figure 5 shows the schematic layout for our proposed spectrometer. The details of the individual components of the system will be discussed in the following sections, here we just wish to describe the general features of the apparatus. For photon detection we have selected a fine-grained liquid-argon calorimeter (LAC). The device will be subdivided into front electromagnetic and downstream hadronic sections, all contained within one dewar. The 3m diameter LAC will have an acceptance of essentially 2π in azimuth and of $\sim$2 units of rapidity, centered at $y_{cm} = 0$ at 530 GeV/c. The detector will subtend an angular range between 22 mr and 167 mr in the laboratory, corresponding to pseudorapidities of 4.5 to 2.5. We have designed the system to provide sufficient coverage in the forward direction in the center of mass so as to accommodate the expected forward peaking of the photon yield in π-nucleon interactions.[14] The overall acceptance of our proposed new

spectrometer is about a factor of 14 larger than that characterizing the geometry of E629. When this factor is combined with the large increase in yield anticipated in going to 530 GeV/c, we expect in excess of 10^4 events with $p_T \gtrsim 5$ GeV/c per 200 hours of π^- running time (in contrast to only a few dozen using the E629 spectrometer). To obtain explicit rates, we employ the specific model used by R. Hagelberg et al. to estimate their yields.[15] This model includes contributions from both $\bar{q}q$ annihilation (both valence and sea quarks) and gq Compton scattering (beam and target gluons added incoherently). Scaling violation is included, but not p_T smearing. (See R. Hagelberg et al.[2] for further details concerning the explicit parametrization of the various structure functions, etc..) Table I presents the model predictions for stated assumptions concerning the experiment. Based on the results of E629, we anticipate that for $p_T \gtrsim 5$ GeV/c the measurement of the difference in the direct γ yield in π^+ and π^- collisions will be limited by statistics rather than uncertaintly in backgrounds from π^o's or η^o's. In Table II we provide an estimate of the fractional error in the difference measurement, assuming for the background a $p_T/\sqrt{s}$ scaling of our results in E629.

We close this overview with the observation that it could undoubtedly be argued that, by ignoring more complicated diagrams which might contribute to the direct photon yield, we are taking an excessively naive view of nature. There is, however, considerable theoretical divergence on this point, with some optimists arguing that higher order graphs will not significantly alter the first order phenomenology.[1] Our position is that this simple model, and our earlier extrapolations, should be adequate to indicate the high quality of the data which we can expect to acquire, and to suggest how valuable these data will be in helping confront some of the most interesting present issues in strong interaction dynamics.

B. Components

The major elements of our proposed experimental arrangement are described in more detail below.

1. The Beam

To achieve our experimental goals, we require a beam capable of delivering $\gtrsim 10^7$ π^- per second within a beam spot of ~ 1 cm^2. The M6 beam could, in principle, satisfy these requirements, but at a perhaps prohibitive cost in proton consumption ($\sim 2 \times 10^{12}$ protons/spill for π^- running). We are therefore investigating the desireability of increasing the M6 flux by about an order of magnitude through widening its momentum acceptance. The upgraded M1 beam in its second phase would also appear to satisfy our requirements. Our proposed π^+ running will pose some additional minor constraints on either beam. With sufficient total flux, selective filtering can be employed to significantly reduce the proton component of the beam[16], but tagging to separate pions and protons will nevertheless be required. An attractive way to proceed, in light of the uniquely high-γ values characteristic of pions in this experiment, would be to build a transition radiation detector, segmented sufficiently to achieve the necessary rate capability. A design along the lines used by L. C. Myrianthopoulos et al[17] in the M6 beam should prove quite acceptable for p/π^+, and possibly for $p/K^+/\pi^+$ separation. (For more discussion see our response to Question 2 from the PAC, June 1981.)

2. Charged Particle Detection

To provide excellent acceptance for studying the fragmentation properties of constituents that are produced in association with direct photons, we require a large-aperture magnet with a moderate field integral of ~ 1 T m. For simulation purposes, we assume that a 72D36 with a vertical gap of ~ 30 in

(or some similar dipole) will be used in E695. In the region in front of the magnet, we plan to install an array of silicon strip detectors.[18] Our present intent is to position 2 such detectors upstream of the target (in an xy orientation), and 6 more immediately downstream of the target (oriented in an xyxyxy sequence). Figure 6 displays a sketch of the proposed arrangement; reports presented at the recent Workshop on Solid State Detectors at Fermilab indicate that these detectors can be positioned within 2 cm of each other without interference between their readouts. We propose to construct each silicon detector with a center-to-center strip separation of $\lesssim$100 μm. This very fine spatial resolution will provide us with an excellent capability for resolving charged-track reconstruction ambiguities, and for determining the interaction vertex and the magnet entrance angle for each secondary track. We anticipate that these devices will not be sufficiently damaged by exposure to radiation during our data taking to necessitate replacement of the silicon wafers.[19]

Downstream of the magnet we will rely on the conventional PWC planes, similar in design to those manufactured at Saclay. We plan to employ 3 independent sets of planes, each capable of generating space points. These chambers will span the beam, and will therefore require desensitized central regions. Our present idea is to achieve this requisite deadening by independent biasing of the cathode pads in the regions in question so as to drive the chambers locally below the point at which positive-ion buildup is a problem. Depending on the actual beam intensity, these central regions may stay partially sensitive ($\sim$50% efficient). Figure 7 displays a sketch of the proposed configuration indicating the orientation angle for each chamber. We believe that the high degree of redundancy provided by our proposed chamber configuration will be essential for disentangling the anticipated high-multiplicity events. We estimate a momentum resolution

of ~10% for charged secondaries of about 100 GeV/c. Above 100 GeV/c, and for neutral hadrons (e.g., K_L^o, n, etc.), the momentum measurement will be obtained using calorimetry, with an expected resolution for hadrons of $50\%/\sqrt{E}$.

Finally, although not specifically addressed in this proposal, we certainly recognize the intrinsic value of secondary particle identification. The spacing of the downstream PWC's can be easily altered to permit the installation of an imaging Cherenkov counter to upgrade our proposed apparatus. At present, we know of no appropriate device that would satisfy, in particular, the intensity and multiplicity requirements of our experiment. We intend, however, to keep abreast of progress in this field and , if appropriate, to initiate a development program of our own in this area.

3. Liquid Argon Calorimeter

A. Photon Detection

As previously stated, the experience we have gained from E629 convinced us that a liquid argon calorimeter will be most appropriate for photon detection. We strongly believe that even a factor of two or three reduction in response time which might be gained through the use of an alternate technology would be outweighed by the excellent linearity, long-term stability and, probably, lower cost of a liquid argon system. We envisage a detector similar in conception to the one employed in E272 and E629, but possessing cylindrical symmetry. Our present plans call for a combined electromagnetic and hadronic calorimeter; the active area would have a 1.5 m outer radius with a beam hole of 20 cm radius, and the entire detector would be installed in a single cylindrical dewar of ∿2.5 m radius. Detailed engineering studies have commenced on the kind of dewar to use and on the question of access to the inside of the dewar (see Appendix B). While access through just

the top will not present us with any new problems relative to those already solved in constructing our present device, it is not clear whether it is technically and economically feasible to equip the dewar with a removable back cover (which would considerably simplify the assembly of the inside detector). In any event, the overall size of the proposed device will clearly be considerable, and may necessitate the construction of a special pit if the experiment is to be installed in the Meson Lab.

In keeping with the choice of cylindrical geometry, we plan to employ an (r,ϕ) readout for the electromagnetic section of the LAC. This will involve the use of g-10 boards with concentric circular strips to measure the radial energy deposition, interleaved with boards etched with radially directed strips to measure the azimuthal variation. The circular strips will typically be 5 mm wide, with their widths increasing somewhat in a gradual fanning out along the axis of the detector (in such a way as to focus the detector on the target). There will be 260 circular strips on each board. It is our present intent to subdivide the radial strips at the mid-radius of the detector. The inner strips will have widths that spread out radially from $\sim$2 mm at the inner edge of the LAC to $\sim$8 mm at a distance of 85 cm from the beam; the outer strips (2 for each inner strip) will vary from $\sim$4 mm to $\sim$7 mm in width. (The strip width will be $\sim$5 mm at a distance from beam center corresponding to $y_{cm}=0$ at 530 GeV/c; the natural size of electromagnetic showers does not, in general, justify a detector granularity finer than $\sim$5 mm.) This proposed segmentation would result in a <u>total</u> of 664 inner strips, and twice this many outer strips. Readout of the inner strips poses a special design challenge which we are still addressing. Should a satisfactory solution fail to emerge, we would propose an alternate subdivision

of the radial strips into two equal area segments both of which can be read out from their outer edges (see Fig. 8). The detector will be subdivided electronically into independent octants for a total of 4072 (or 3408) channels in its front section. The electromagnetic section of the detector will be subdivided into two 9 radiation-length sections along the beam direction; the r-strips in the upstream unit will be connected to TDC's to obtain $\lesssim$6 ns time resolution for energy deposition. To reduce the total number of amplifier channels required, the downstream section of the detector can be constructed using strip widths twice those of the front section. This will not compromise the angular resolving power of the detector. A sketch of the active area of the proposed detector is presented in Fig. 8.

The large size of the photon detector has been dictated, in part, by our desire to sample the neutral (π^0) energy accompanying the direct photon. This information, combined with that from the other components of the spectrometer, will be vital for extracting details of the gluon fragmentation process, one of the major goals of this experiment.

B. Hadron Calorimetry

To maximize the acceptance of our spectrometer for particles produced in the fragmentation of constituents, we plan to use a magnet that provides a rather small transverse impulse ($\sim$250 MeV/c). This choice, naturally, compromises somewhat the measurement of charged tracks with momenta $\gtrsim$100 GeV/c. To circumvent this deficiency, and to be able to measure neutral hadron energy deposited in the 22 mr to 167 mr range of laboratory angles, we propose to build the LAC with two hadronic layers following the two relatively thin electromagnetic sections. The inherently large transverse dimensions of hadronic showers obviate the need for having

the kind of fine-grained segmentation used in photon detection. We therefore plan to build a device that will have a pad (rather than strip) read out for both hadronic sections. The smallest pads, near the center, will have areas of $\sim 30\ cm^2$, the largest (at the outer edge) will have areas of $\sim 150\ cm^2$. The pads will, of course, be focussed towards the target in the same way as the strips are in the electromagnetic front sections. (The details of the readout and construction can be found in Appendix B.)

Although one of the main reasons for subdividing the hadronic section of the LAC into two separate units ($\sim$3.5 interaction lengths each) is dictated by the need to maintain as small a capacitance per channel as is possible, we believe that this separation will also serve to improve energy resolution for electromagnetic showers that penetrate through the first 18 radiation lengths of the LAC; in addition, we expect to obtain better spatial localization of hadrons as a result of this forward/backward segmentation of the hadronic part of the LAC. The pad type of read out should also prove to be valuable in dealing with pattern recognition problems originating both in the electromagnetic part of the LAC, as well as in the charged-particle reconstruction using the PWC system.

4. Target Selection

The proposed $\pi^+ - \pi^-$ difference measurement for obtaining the contribution of the annihilation diagram does not have to be restricted to the case of nuclear targets. In fact, the difference per nucleon (ignoring $\bar{q}$ contributions from the sea) is a maximum (by a factor of 2) in the case of hydrogen. Nuclear targets do however have the virtue of being compact and easy to handle, and moreover the use of an I=0 target such as carbon has the important added advantage of eliminating any residual π^o and η^o background through the $\pi^+ - \pi^-$ subtraction; looked at from another point of view, comparison of π^o and η^o production provides an excellent internal check on

the presence of any systematic differences between the π^+ and π^- running. We therefore propose to employ a 10% absorption length carbon target for most of our data taking; for comparison purposes, we will replace this with similar beryllium and aluminum targets for part of the run.[20] We reserve as a future option the installation of a liquid hydrogen target; to achieve the same level of sensitivity, this would necessitate raising the beam intensity by a compensating factor of $\sim$3.

5. Experimental Trigger and Backgrounds

One of the primary goals of our test experiment E629 was to investigate these two important topics. The E629 trigger involved specially constructed modules which enabled us to establish independent triggering thresholds for the total transverse energy deposited in the LAC (global p_T), and for the peak transverse energy deposited in 3 adjacent strips (local p_T). Although we had a rather limited amount of beam time, we were, nevertheless, able to investigate the crucial factors that must be taken into account in any successful attempt at executing a direct-photon experiment. (We discuss our experience in the attached Appendix A.) As just one example, we cite that setting the local p_T threshold to $\sim$1/3 that of the global threshold is vital for reducing background at the trigger stage. It is worth emphasizing that, relative to E629, background rates at higher p_T in E695 should be considerably reduced and, moreover, the cylindrical geometry chosen for our new LAC should be more ideally suited for the type of global-p_T/local-p_T fast logic than we used in E629.

6. Forward Hadronic Calorimeter

Charged particles produced with $p_T \gtrsim 2$ GeV/c at forward angles of $\lesssim$20 mr (as well as neutral hadrons at small angles) will miss the acceptance region

of the LAC. Consequently, the energy information for these particles will either be unavailable or compromised. We therefore plan to install a small ($\sim \frac{1}{2}$ m^2 area by $\sim$8 interaction lengths) hadron calorimeter, that will have a granularity of $\sim$40 cm^2, and place it just downstream of the LAC. This device will have a beam hole of $\sim$5 cm in diameter and it will overlap somewhat the acceptance at the inner edge of the LAC.

This forward calorimeter will provide us with a capability for investigating correlations between the break up of the unscattered-beam constituents and the characteristics of the triggering collision at large p_T. In addition, the calorimeter will be valuable in sharpening the momentum resolution in the measurement of the more energetic constituent fragments emitted at angles $\lesssim$20 mr. A sketch of a possible design of such a device is given in Appendix C.

III. ACCEPTANCE AND RESOLUTION OF SPECTROMETER

A. LAC

The anticipated acceptance and resolution of the LAC can be summarized as follows:

1) For electromagnetic showers:

Energy $\frac{\Delta E}{E} \sim 14\%/\sqrt{E}$

Positional $\sigma_x \sim 0.7$ mm

Directional Resolution $\Delta\theta \sim 25$ mr

Temporal Resolution $\sigma \sim 6$ nsec

2) For hadronic showers:

Energy $\frac{\Delta E}{E} \sim 50\%/\sqrt{E}$

Positional $\sigma_x \sim 3$ cm

The effective acceptance of the LAC for direct photons extends from 25 mr to 164 mr, corresponding to a rapidity interval of $\sim$2 units, centered on $y_{cm}=0$ at 530 GeV/c. (See Appendix A for a justification of the electromagnetic parameters.)

B. Forward Hadronic Calorimeter

The effective acceptance extends from 5 mr to 26 mr. Positional and energy resolutions comparable to that of the LAC.

C. Magnetic Spectrometer

In the calculation of the acceptance and resolution we have assumed the availability of 72D36 magnet with a vertical gap of 30 inches, and an integrated $B \cdot \ell$ corresponding to a transverse impulse of 250 MeV/c. Figure 9 shows, for charged pions, regions of > 90% and > 50% efficiency in both $y_{cm} - p_T$ and $x_F - p_T$ space. It can be seen that for all but the lowest p_T values, the spectrometer cuts off at a fixed cm angle (corresponding to the Lorentz transformed aperture of the magnet). For this reason, the angular variable y_{cm} is a somewhat more natural choice than x_F for analyzing the acceptance. In Figure 10 we display the spectrometer acceptance vs. rapidity for representative p_T values for each secondary particle species. As p_T is increased, the various curves approach a common asymptote corresponding to the spectrometer's minimum acceptance of ~94% of the total cm solid angle. Many of the interesting questions concerning parton fragmentation involve the characteristics of the leading fragmentation products. In Figure 11 we display our acceptance for the leading and next-to-leading charged fragment of a parton recoiling from a direct photon. The curves are presented as a function of the rapidity of the fragmenting parton for γ triggers of 5 and 8 GeV/c. (We employed the Feynman-Field parameterization to describe the fragmentation process.)

It is clear that the proposed spectrometer system will have excellent acceptance. We will therefore be able to examine in substantial detail the nature of constituent fragmentation.

IV. SUMMARY

We propose to investigate the detailed characteristics of events which have direct photons produced at large transverse momenta in hadron-nucleon collisions. At large values of p_T, the photon yield is expected to be comparable to that for π^o and η^o production. The fine-grained photon detector which we propose to construct will provide excellent γ/π^o discrimination. The π^o, η^o and ω^o yields (interesting in their own right) will be measured with precision and used to subtract remnant background from the observed single photon signal. Comparison of the yields for π^+, π^- and p projectiles in a single experiment over a wide range of rapidity will permit us to extract the gluon structure function for these hadrons, and also to analyze the fragmentation properties of quarks and gluons. Data that will be obtained on direct two-photon production will provide further information on the gluon content of hadrons, and will also serve as a new and important testing ground for QCD. In addition, the large acceptance and excellent resolution of our proposed spectrometer will enable us to search for possible new massive meson states (glueballs, etc.) produced in hadronic interactions.

The cost of mounting this experiment will be of the order of $2.6M; a more detailed breakdown of the estimated expenses is given in Appendix D. We have enlarged the membership of our collaboration so as to be able to construct the equipment on a time schedule in line with the expected turn-on of the Tevatron. We anticipate a 2 to 3 year construction schedule for the major components of the apparatus.

FOOTNOTES AND REFERENCES

(1) An excellent summary of the physics possibilities is offered by F. Halzen and D. M. Scott, Madison Report DOE-ER/00881-15G (1980). In remarkably enthusiastic fashion these authors sketch why direct photons is "the way" to do high-p_T physics with hadrons.

(2) L. Bachmann et al., Geneva-Neuchatel Collaboration, CERN/SPSC/80-61 (1980);

A. Bamberger et al., Bari-Freiburg-ITEP Moscow-Max Planck Inst.-Munich-Nijmegen Collaboration, CERN/SPSC/80-83 (1980);

R. Hagelberg et al., CERN-Saclay-Collège de France-Ecole Polytechnique-Orsay-Pisa Collaboration, CERN/SPSC/80-109 (1980);

J. Antille et al., CERN/Lausanne/Michigan/Rockefeller Collaboration SPSC/80-63 (1980).

(3) See Ref. 1 and previous work referred to in that paper. Also, the proposal of R. Hagelberg et al. (Ref. 2) has detailed comparisons of the contributions from the various graphs.

(4) B. L. Combridge, CIT Report CALT-68-766 (1980).

(5) Private communication. We thank Dr. Petronzio for a helpful and encouraging discussion. See also A. Kotanski and J. Kubar, Acta Physica Polonica B11, 669 (1980).

(6) See M. Diakonou et al., Phys. Lett. 91B,296 (1980), and reference to previous work given therein and in our earlier proposal (E629) to Fermilab.

(7) Private communication from W. Molzen from ISR experiment R807, and from L. Camilleri of the CCOR group. See also the latest data and theoretical comments contained in the summary of the CERN Discussion Meetings Between Experimentalists and Theorists on ISR and Collider Physics, Series 2, Number 1 (1980), M. Albrow and M. Jacob, eds.

(8) Private communication from N. Giokaris.

(9) See the remarks of S. Brodsky in his lectures at the 1979 SLAC Summer Institute, SLAC-PUB-2447 (1979), and the work of M. Creutz, Phys. Rev. D21, 2308 (1980).

(10) See Ref. 4 and C. Carimalo et al., Phys. Lett. 98B, 105 (1981). Carimalo et al. stress the importance of the two photon measurement, particularly with regard to the extraction of the gluon structure function of hadrons via the process $gg \rightarrow \gamma\gamma$. See also reference to earlier work given in these two papers.

(11) It is interesting to note that the latest data from the R807 group at the ISR provides an indication for the presence of a two-photon signal in pp collisions. The order of magnitude of the yield is consistent with expectations from antiquarks from the sea. The data are not yet sufficiently refined to shed light on the $gg \rightarrow \gamma\gamma$ question. We thank Dr. I. Stumer of BNL for a valuable discussion of the latest data and phenomenology and for providing us with a copy of E. Paschos' report (early 1970's) on massive photon pairs.

(12) Dr. C. A. Nelson of SUNY Binghamton is presently examing this problem.

(13) R. P. Feynman and R. D. Field, Nuc. Phys. B136, 1 (1978).

(14) The peak of the photon yield is expected to occur between 1/3 and 1/2 rapidity units forward of $y_{cm}=0$. For explicit calculations demonstrating this effect, see R. Hagelberg et al., Ref. 2.

(15) We thank J. Badier for providing us with detailed calculations for our energies. Our use of the Hagelberg et al. model to calculate our yields has the advantage of facilitating comparison between our experiment and theirs. The rates based on this model are similar to those predicted by B. L. Combridge, Ref. 4.

(16) During our 1979 data run for experiment E272, we successfully employed a beryllium filter to enhance the kaon fraction of our 200 GeV/c positive beam without observing significant deterioration in our Cherenkov tagging efficiency. Using 2.2 m of Be, we were able to change the beam composition ($p:\pi^+:K^+$) from (.81:.16:.03) to (.29:.51:.20). For further details, see A. Jonckheere et al., NIM 180, 25 (1981).

(17) L. C. Myrianthopoulos et al., Maryland Report ORO 2504-320 (1980). Also see Appendix A of proposal for E672.

(18) Great progress has recently been made in the development of such detectors at CERN; e.g. the report of E. H. M. Heijne, et al., Nucl. Instr. and Meth. 178, 331 (1980). The CERN-Munich collaboration (B. Hyams et al.) is presently preparing a 1000 channel system for use at high intensities during the 1981 Fall SPS running period. Members of our collaboration are presently actively investigating such detectors at Fermilab.

(19) Current estimates are that such detectors can withstand an integrated flux of 10^{14} charged particles per cm^2. See the report of Ref. 18 and T. Ludlam's summary at the Pisa Conference on the Miniaturization of Detectors (1980) for further details. In any event, the cost of the silicon wafer is expected to be small compared to the cost of the accompanying electronics.

(20) It has been pointed out to us by E. Berger that measuring the inclusive γ cross section as a function of atomic number would shed light on the question of higher twist contributions in QCD. Consequently, it appears that measurements using various nuclear targets might be important in their own right.

Table I

Expected Yield of Direct Photons

Number of Events per 1 GeV/c Interval in p_T

p_T (GeV/c)	$\pi^- C$ (500 hrs at 530 GeV/c)		$\pi^+ C$ (700 hrs at 530 GeV/c)		pC (400 hrs at 800 GeV/c)	
	[γ]	[γγ]	[γ]	[γγ]	[γ]	[γγ]
5	34,000	330	34,000	120	29,000	90
6	9,500	90	9,000	40	6,000	20
7	2,500	26	2,100	11	850	3
8	650	8	450	3	160	
9	180	3	120	1	40	
10	50	1	25		7	
11	12		5		1	

The numbers in this table were obtained using our acceptance and the model of Hagelberg et al (references 2, 15). We assumed 10^7 beam/sec for incident pions, and 1.5×10^7 beam/sec for incident protons. A 10% absorption length target was assumed, and a 25% duty factor for the Tevatron. The columns labeled [γ] are for a single photon in the indicated p_T range; the columns labeled [γγ] are for two photons in our range of acceptance and at least one within the given p_T range. The single γ yields for 400 hours of running at 400 GeV/c, for pC collisions, will be ∿ 6000, 900, 80 and 5 events for p_T values of 5, 6, 7 and 8, respectively.

Table II

Fractional Error Expected on Difference in Direct Photon Cross Section for π^+C and π^-C at 530 GeV/c.

p_T (GeV/c)	$\delta(\Delta\sigma)/\Delta\sigma$ (For 1 GeV/c Intervals)
5	0.03
6	0.05
7	0.07
8	0.10
9	0.14
10	0.27
11	0.50

The calculation assumes a $p_T/\sqrt{s}$ scaling of the background observed in E629. For comparison, Hagelberg et al.[2] expect an error of 0.19 in their determination of $\Delta\sigma$ for $p_T > 5$ GeV/c.

Figure Captions

1. Elementary diagrams contributing to the direct photon signal in hadronic collisions. (Permutations and exchange graphs for the indicated processes are not explicitly shown.)
2. Measured energy dependence for π^o production in pp collisions for representative values of p_T. Curves are normalized to the yield at 200 GeV/c.
3. Transverse momentum dependence of the relative yield of π^o mesons in $\pi^- p$ collisions. The increase of the π^o yield between 200 GeV/c and 530 GeV/c has been estimated using an extrapolation from measured $\pi^\pm$ data; see text for explicit details.
4. Elementary diagrams contributing to the production of two direct photons. The Drell-Yan diagram is shown for comparison purposes. (Permutations and exchange graphs for the indicated processes are not explicitly shown.)
5. Schematic layout of our proposed experimental arrangement.
6. Enlarged schematic view of the target region indicating areas and orientations of individual elements. Angle values denote strip orientations relative to 0° for a vertical strip (corresponding to readout of the horizontal coordinate).
7. Enlarged schematic of downstream proportional system indicating orientations of individual chambers and their approximate dimensions. Angle values denote wire orientations of u and v planes relative to 0° for a vertical wire.
8. General features of the proposed electromagnetic part of the LAC. For a description of the hadronic part of the detector and of the dewar see Appendix B. See text for further details.
9. Regions of > 90% and > 50% acceptance for the magnetic spectrometer.

10. Acceptance for different charged particles, as a function of rapidity, for representative values of p_T.

11. Acceptance efficiency for observing the leading and next to leading charged recoil fragment opposite a direct photon as a function of the rapidity of the fragmenting constituent. (Fragments generated using the Feynman-Field ansatz.) Part (a) is for γ triggers at $p_T = 5$ GeV/c and (b) is for triggers at $p_T = 8$ GeV/c.

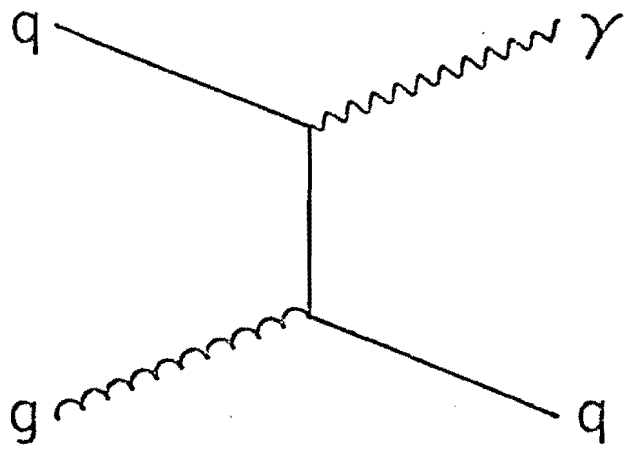

"COMPTON" PROCESS

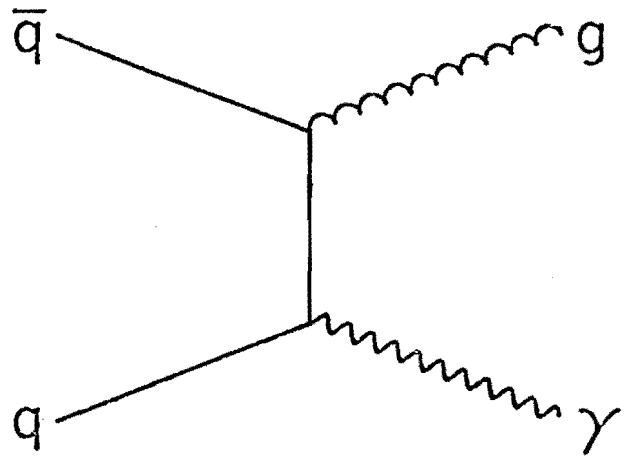

ANNIHILATION PROCESS

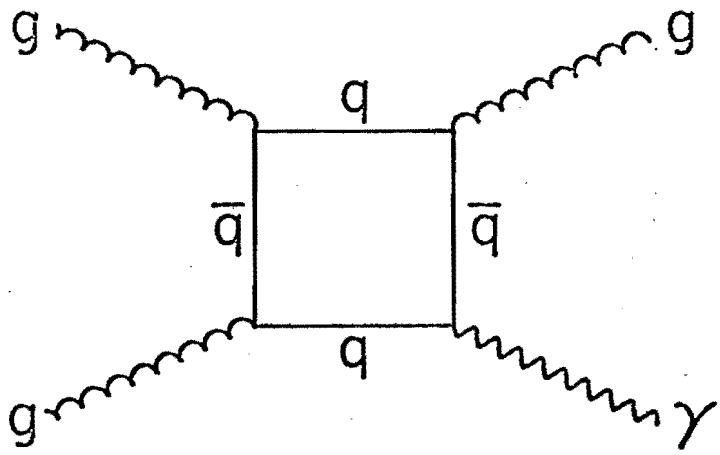

FOUR-QUARK BOX DIAGRAM

Fig. 1

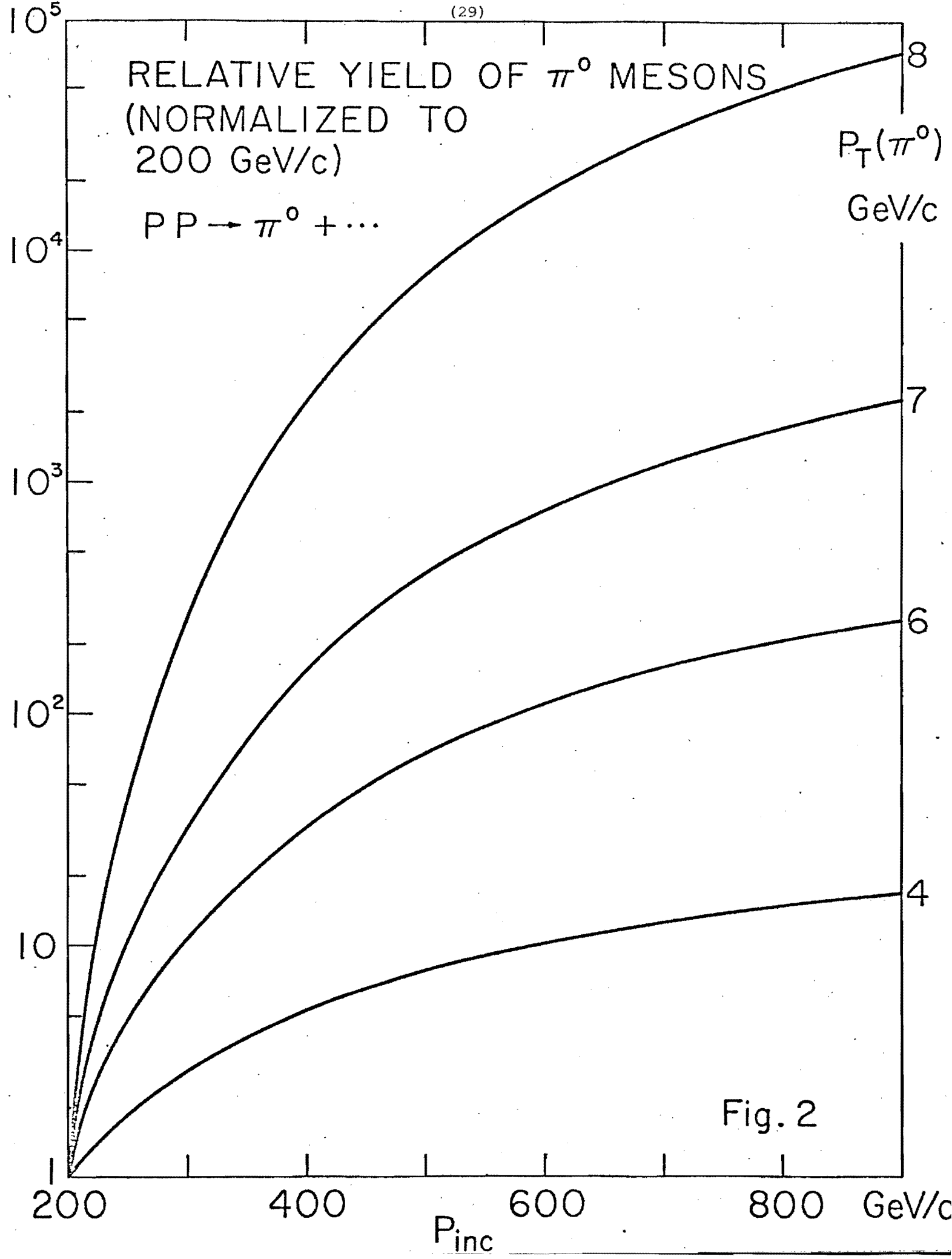
RELATIVE YIELD OF π^0 MESONS
(NORMALIZED TO
200 GeV/c)
$PP \rightarrow \pi^0 + \cdots$
$P_T(\pi^0)$
GeV/c
8
7
6
4
10^5
10^4
10^3
10^2
10
1
200
400
600
800
GeV/c
P_{inc}

Fig. 2

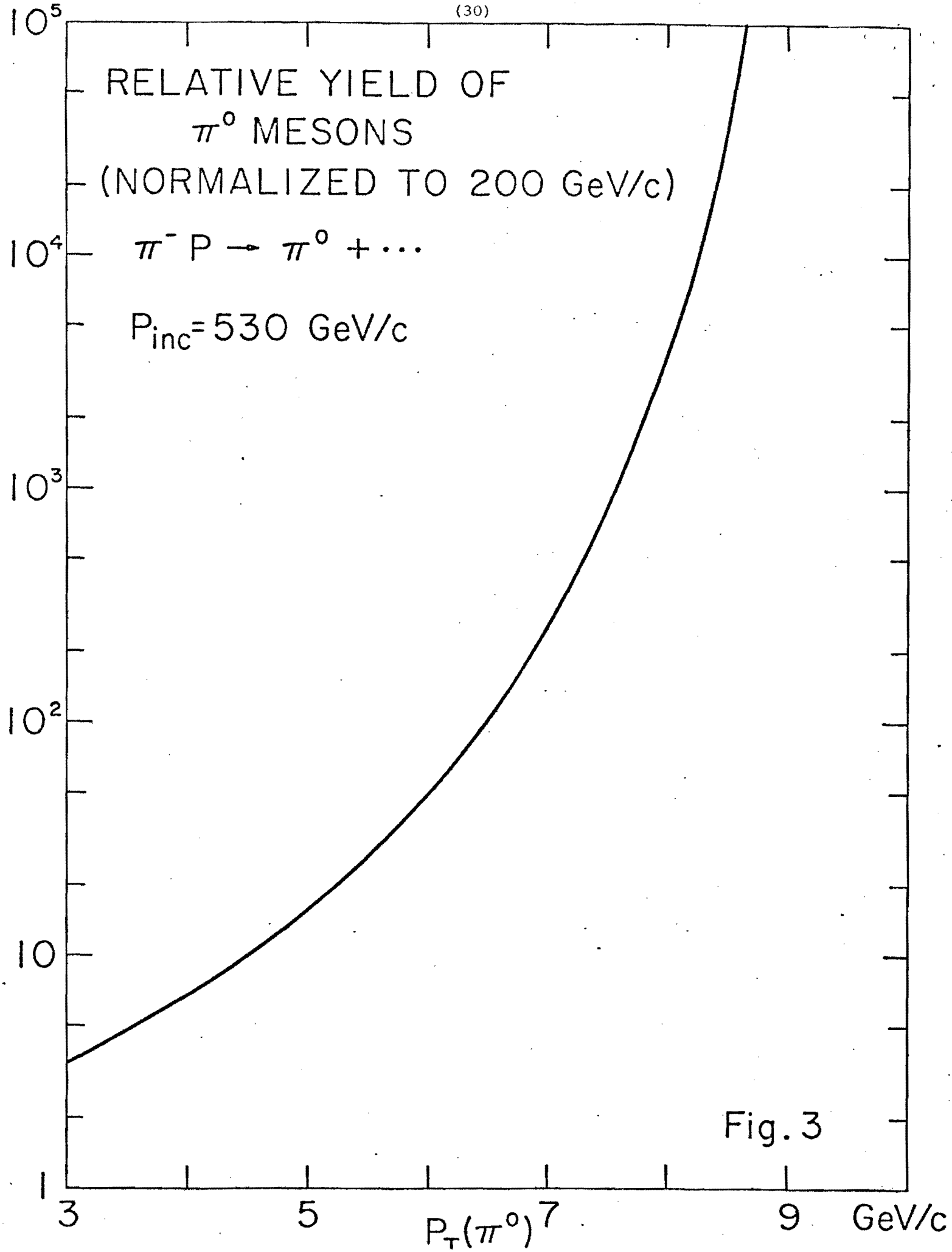
RELATIVE YIELD OF
π^0 MESONS
(NORMALIZED TO 200 GeV/c)
$\pi^- P \rightarrow \pi^0 + \cdots$
P_{inc}= 530 GeV/c
10^5
10^4
10^3
10^2
10
1
3
5
7
9
GeV/c
$P_T(\pi^0)$

Fig. 3

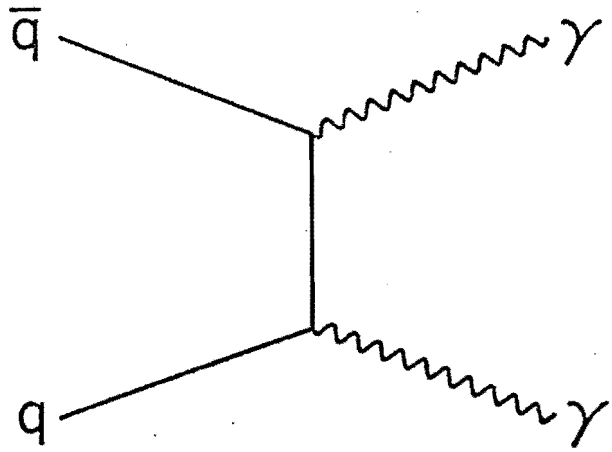

ANNIHILATION PROCESS

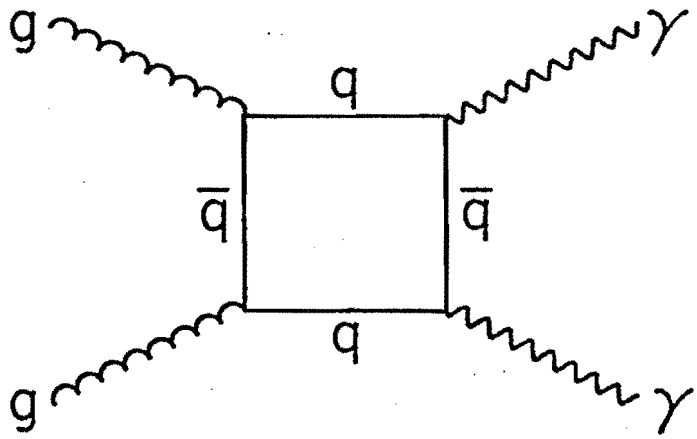

FOUR-QUARK BOX DIAGRAM

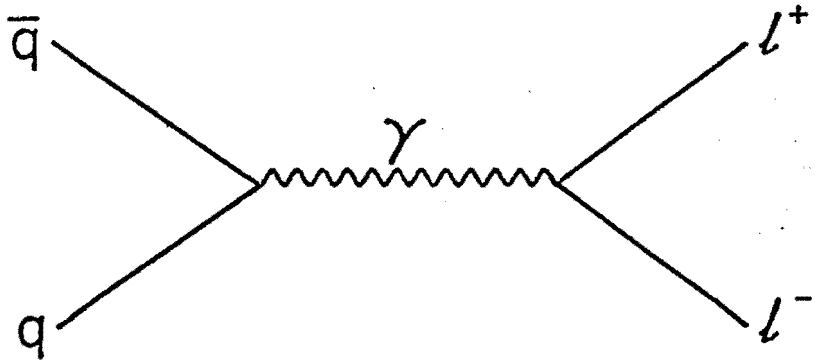

DRELL-YAN PROCESS

Fig. 4

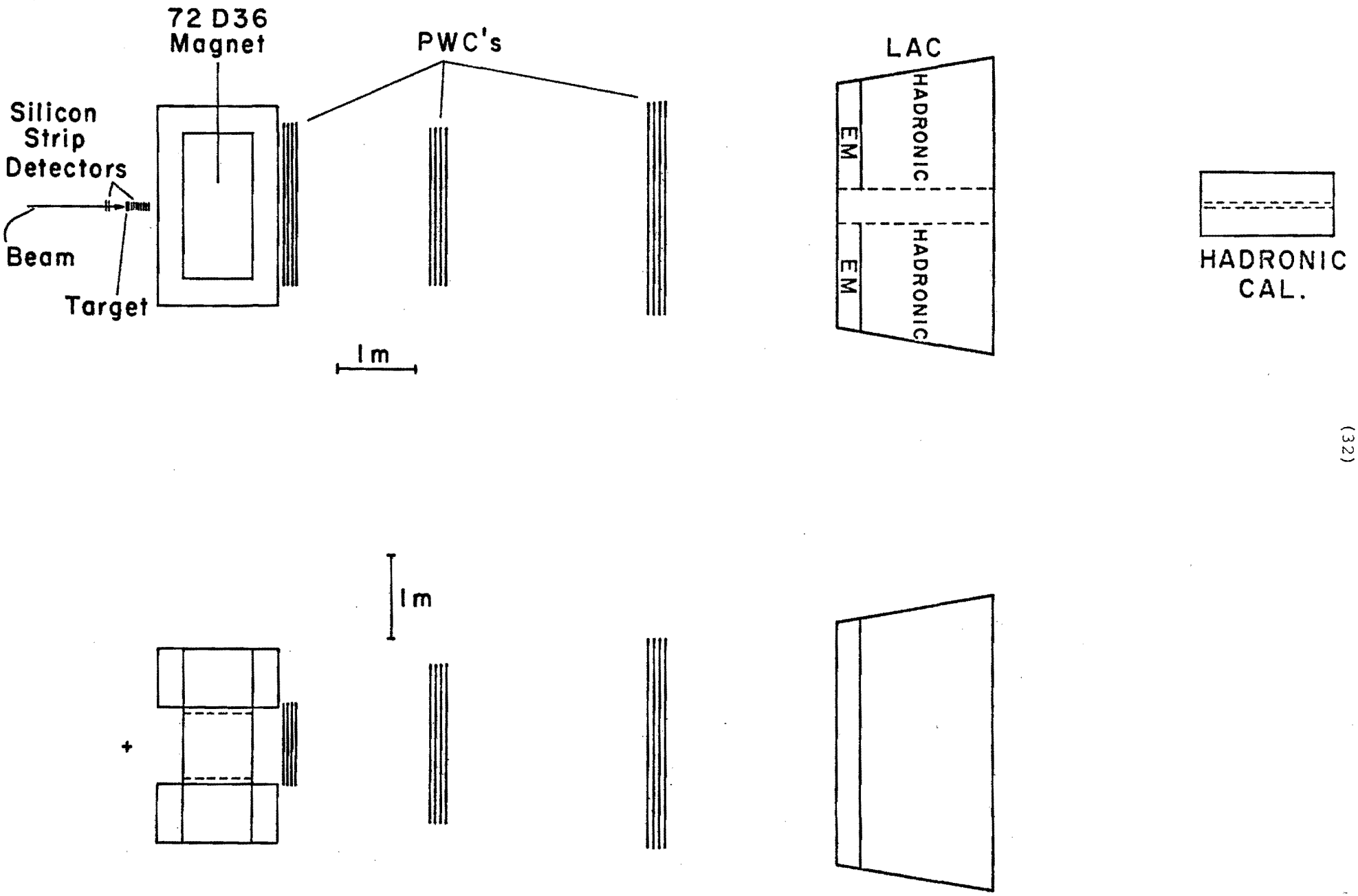

EXPERIMENTAL LAYOUT

Fig. 5

DETAIL OF TARGET REGION

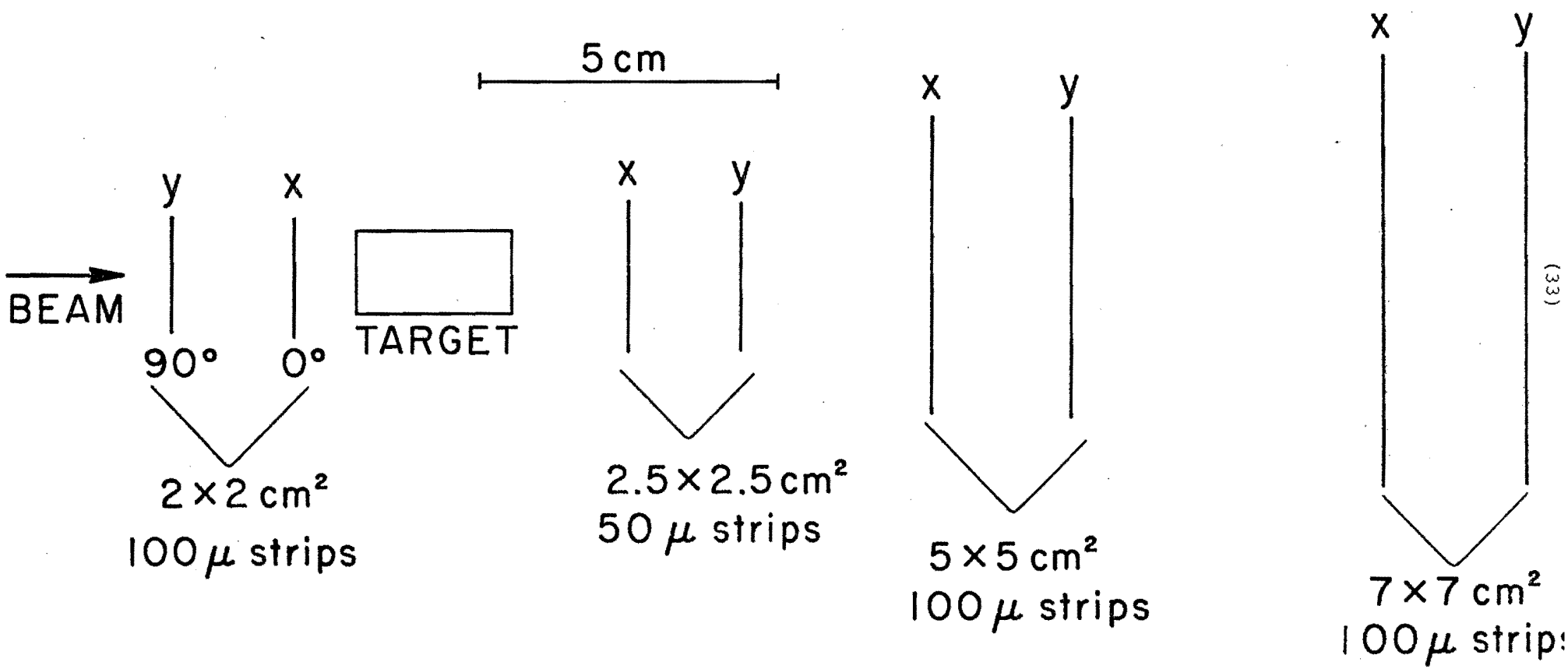

Fig. 6

DETAILS OF PWC SYSTEM

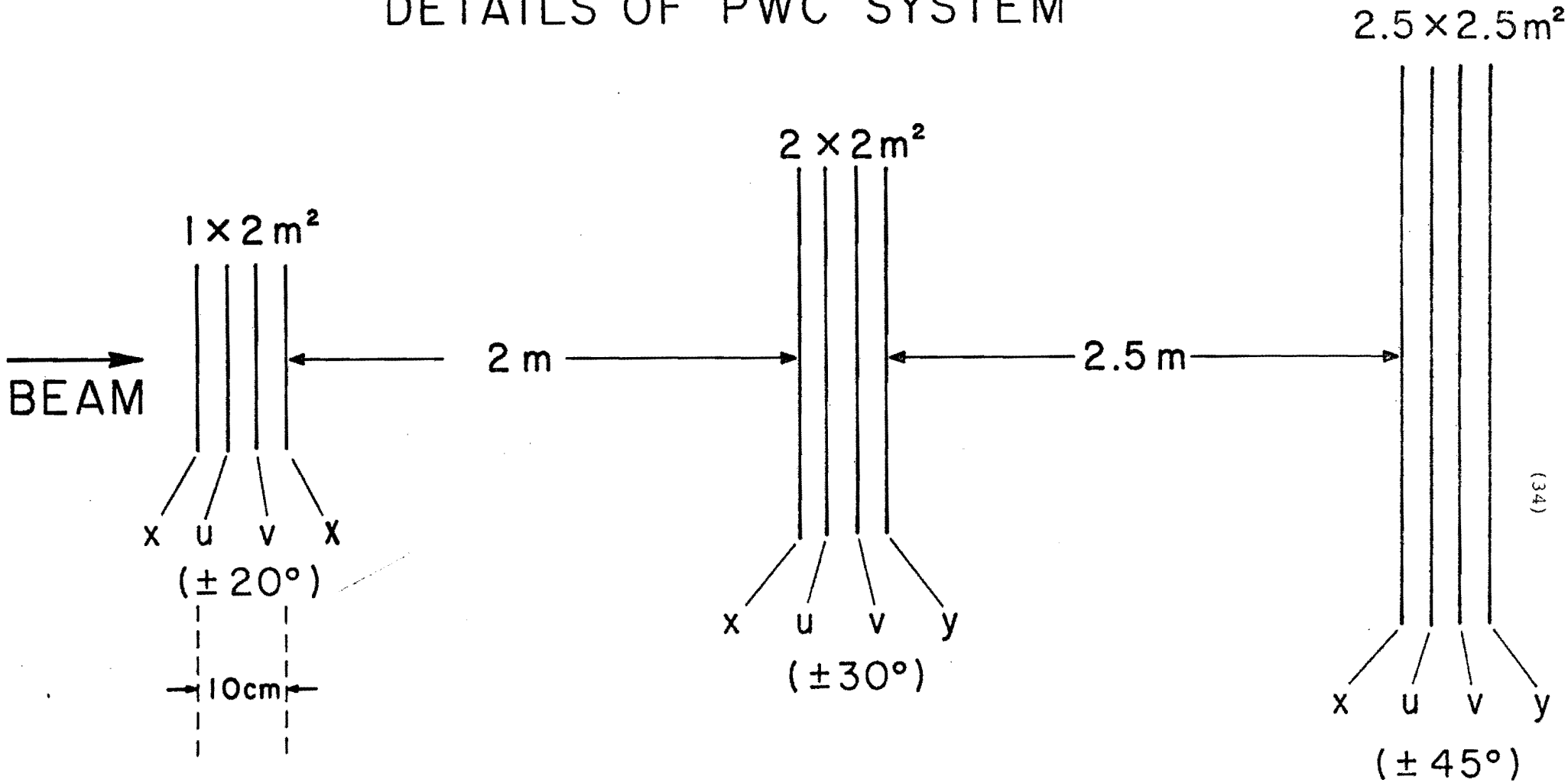

Fig. 7

GENERAL FEATURES OF LAC DESIGN

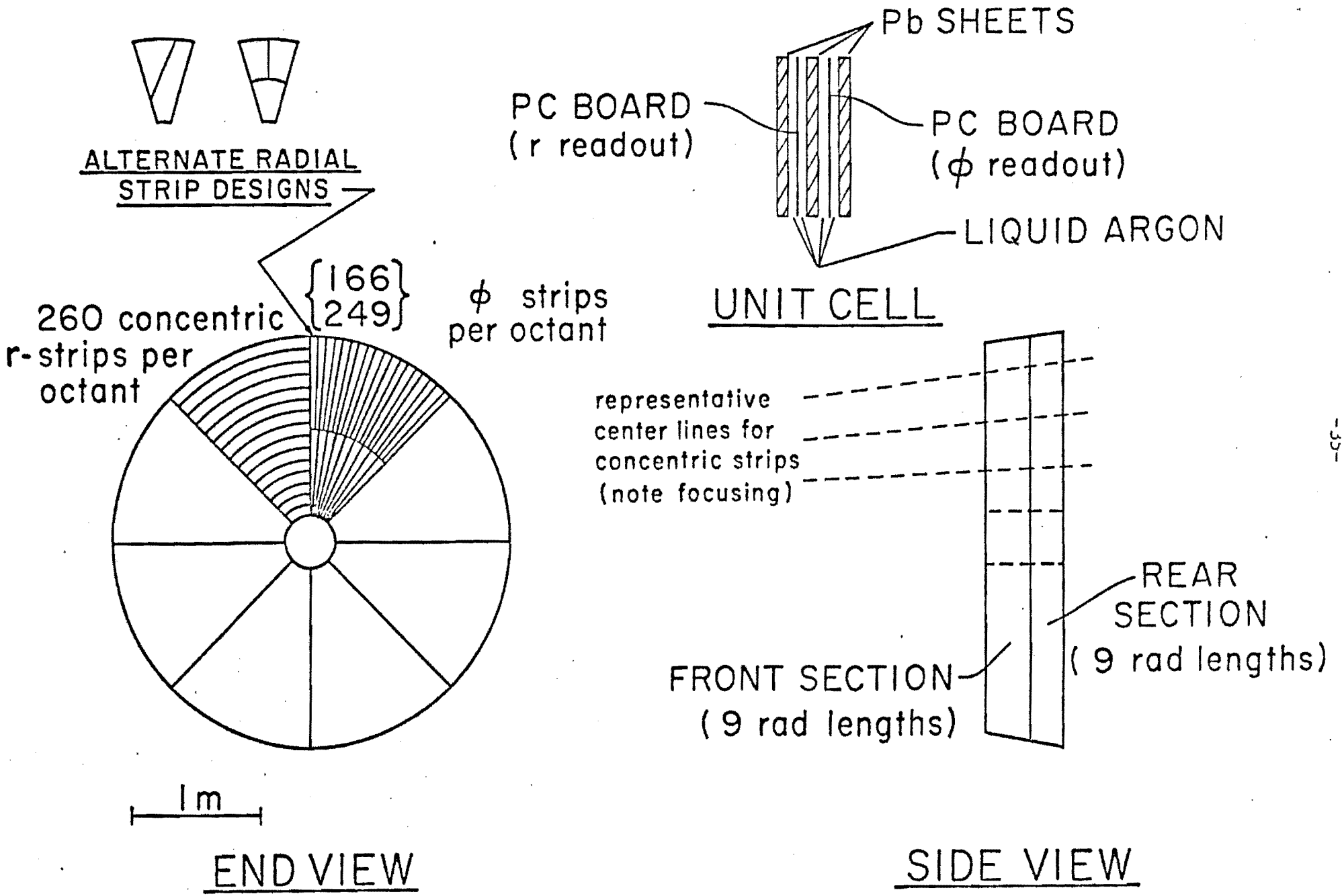

Fig. 8

SPECTROMETER ACCEPTANCE FOR CHARGED PIONS

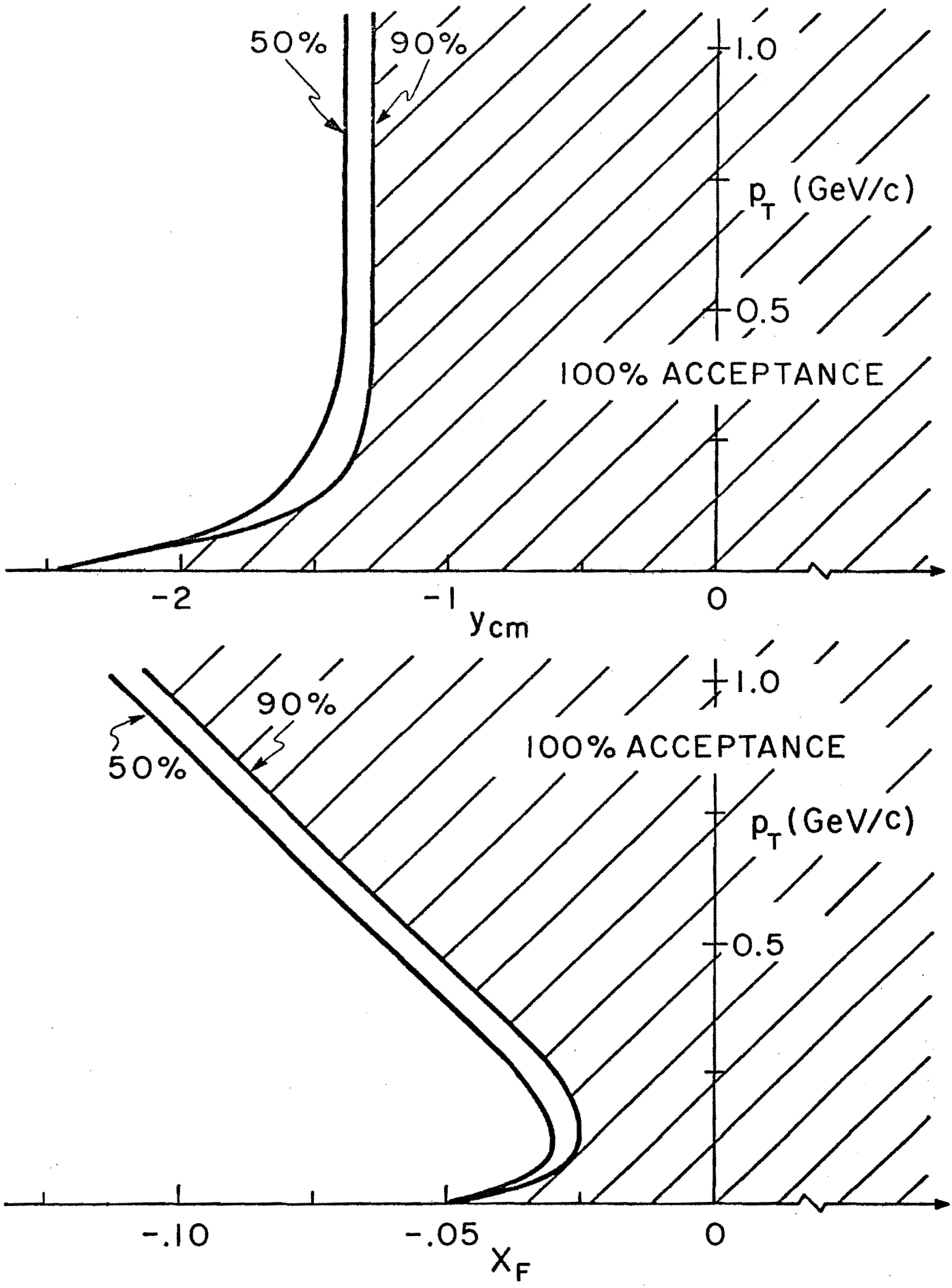

Fig. 9

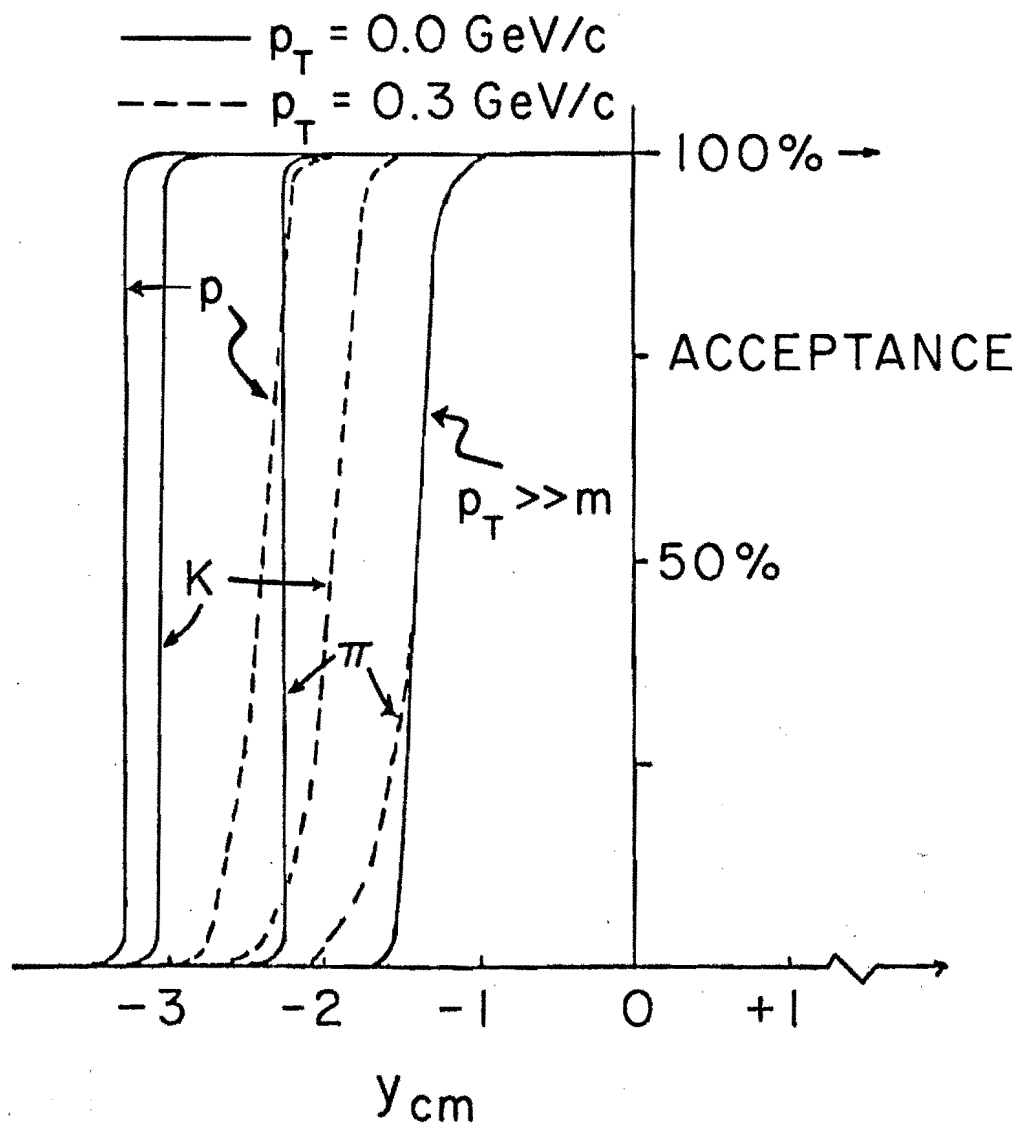

Fig. 10

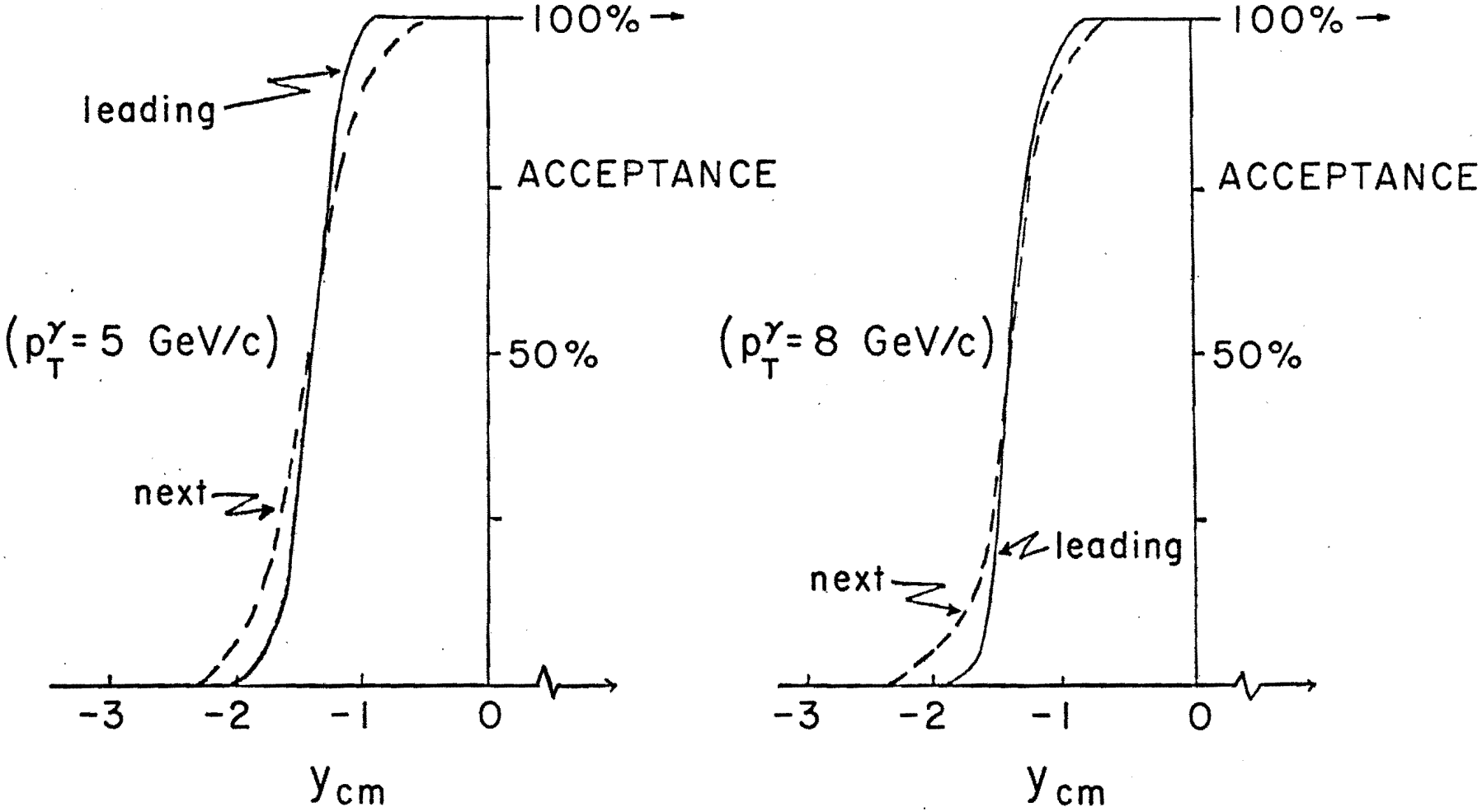
100% →
ACCEPTANCE
50%
leading
next
(p_T^γ = 5 GeV/c)
-3
-2
-1
0
y_{cm}
100% →
ACCEPTANCE
50%
leading
next
(p_T^γ = 8 GeV/c)
-3
-2
-1
0
y_{cm}

Fig. 11

APPENDIX A

Experiment E629 was approved as a test to investigate the problems to be encountered in executing an experiment to study high p_T direct photon production. In particular, we wished to determine the feasibility of employing a LAC in such an investigation. The experiment was setup during the fall of 1980 (the E272 apparatus had by that time been completely removed from the beam line), and the data on which we will be reporting were acquired during the rather abbreviated period of stable Meson Lab operations that winter.

In Fig. 1 we present the layout of the experimental apparatus. The LAC was positioned $\sim$8m downstream of the targets, with its center $\sim$1m from the beam line; in this position it subtended $\sim$1.4 units of rapidity and, for a typical photon, covered $\sim$12% of the azimuth.

The principal questions which we hoped to address via E629 can be summarized as follows:

(1) Can a LAC, which is intrinsically a 3-4 MHz device, be used effectively at a 1 MHz interaction rate?

(2) Can a satisfactory high p_T trigger be implemented?

(3) Can the experimental backgrounds be identified, and either removed and/or corrected for?

(4) Can high associated particle multiplicities be tolerated?

(5) Would there be any unpleasant surprises?

We will examine each of these questions in some detail.

(1) We routinely ran E629 at beam intensities $\gtrsim 10^7$ pps. Rate dependent effects were successfully eliminated via pileup vetoes which protected against the situation in which an apparent high p_T event was in reality the superposition of two successive lower p_T interactions. The presence of these vetoes resulted in an overall dead-time of ∿30%. We estimate that by replacing our slower LAC amplifiers with the current model[1], and by the addition of methane to our argon, we could have reduced this deadtime by about a factor of two; our request for an additional week of running time to experimentally investigate the efficacy of adding methane to our large detector was denied. (Prior to the running of E629, we tested the effects of methane doping using a small test detector, and determined that the addition of ∿1% methane results in a factor of 2-3 improvement in the rise time at the cost of a pulse height dimunition of 20-30%.)

(2) For the purposes of E629 we designed and built special trigger modules which were cabled to the fast outputs of the LAC amplifiers. These modules were designed to perform the following functions:

(a) From a suitably weighted sum of the individual channel outputs, calculate the total (global) p_T deposited in the LAC:

$$p_T^{global} \equiv \sum_i \alpha_i E_i^X + \sum_j \beta_j E_j^Y$$

where α_i and β_j are primarily geometric factors (see, however, the discussion below).

(b) Calculate a local p_T defined in terms of the energy deposited in three contiguous X strips:

$$p_T^{local} \equiv \text{Max} \left(\sum_{i-1}^{i+1} \alpha_i E_i^x \right)$$

(c) Establish, when used in conjunction with our LeCroy 2770 TDC's from E272, the time of the initiation of the energy deposition in the front strips of the LAC.

The role played by the local p_T requirement in our trigger can be understood as follows. By requiring that, in addition to a global p_T trigger, $p_T^{local} \gtrsim \frac{1}{3} p_T^{global}$, one can essentially eliminate triggers arising from either "coherent noise" (i.e. noise which is common to all of the LAC channels; e.g. SCR pickup from magnet power supplies) or from multi (low p_T) photon induced events. Indeed, we are convinced that such a requirement is an absolutely essential component of any efficient p_T trigger. The TDC timing information enabled us to eliminate off-line those showers which were out of time with the primary interaction; this proved to be very useful in discriminating against beam halo induced accidentals (see below).

The overall sharpness of our p_T trigger is shown in Figs. 2 and 3, where we present the efficiency of our global p_T trigger for π^o's and single photons, respectively; the trigger efficiency was determined from data taken using a (prescaled) trigger of lower threshold for which the result of the normal p_T trigger was merely latched. The data are from the right side of the detector only; the motivation for imposing this cut can be understood as follows.

If the ballast capacitance of the detector is not infinitely large compared to the capacitance of the signal strips to the lead plates, an image charge, proportional to the energy deposited in a given strip, will be formed on all of the other strips. Due to the different weighting factors applied to each strip in forming the p_T trigger, the effect of these image charges on the effective p_T threshold will vary over the

face of the detector. This may be compensated for by modifying the factors α_i and β_j appropriately. This effect was noticed during the early stages of E629, and compensating factors introduced. However, the factors employed were not completely adequate, and there remained a residual variation of the effective p_T threshold across the detector; the p_T threshold on the right 3/4 of the detector was determined to be $\sim$2.4 GeV/c, while that on the left 1/4 was $\sim$3.2 GeV/c. (The need for an additional rescaling of the p_T module attenuators was in fact noted during the E629 data taking; however, retuning these attenuators absorbed nearly two shifts, so, in light of the very tight running schedule, we elected not to retune.) With the proper attenuation factors, Figs. 2 and 3 would have applied over the entire face of the detector; in the case of our proposed new LAC, we intend to increase the size of our ballast capacitors to minimize the overall effect.

We have also analyzed the detailed shape of the p_T trigger threshold, and have found it to be completely consistent with the measured noise in the trigger circuitry. In its totality, our analysis of our E629 trigger has satisfied us that the same general scheme would be entirely adequate for E695.

(3) In discussing the experimental backgrounds encountered in E629, it is important to bear in mind that a prompt photon experiment is equivalent to a good π^o and η^o inclusive experiment, particularly at moderate values of p_T. Thus we begin by discussing our data on these latter processes. It should be noted at the outset that, for the purposes of this appendix, all data displayed have been restricted to an especially clean sample of events to which the following cuts have been applied:

(a) No additional γ's, besides those under investigation, were observed in the LAC. This cut was applied regardless of whether these additional "photons" were ultimately rejected by subsequent cuts (hadron, timing, or directionality). We emphasize that only $\sim$20% of our triggers arose from the 1γ and 2γ events on which we will mainly be concentrating our attention (we will briefly discuss the higher multiplicity events later in this appendix); this fact should be kept very much in mind when interpreting our present results.

(b) The energy of any residual uncorrelated peak in any single view did not exceed 600 MeV. This cut was imposed to eliminate events for which the LAC reconstruction program may have failed (600 MeV equals half the 1.2 GeV cut ultimately to be imposed on all single photons). This cut eliminated only $\sim$2% of the 1γ and 2γ events (it had the same effect on each sample); this is consistent with the $\sim$99% efficiency found for the present version of our reconstruction program (based on a $\sim$35K sample of Monte Carlo generated π^0's).

In Fig. 4 we display the 2γ mass spectrum in the π^0 and η mass regions. The signal-to-background in each case is clearly excellent. The widths (standard deviations, calculated using $\pm 2\sigma$ bands) of the peaks are 6.5 MeV (π^0) and 17.5 MeV (η), respectively. These values are nearly identical to those which we obtained previously in E272, and attest to the remarkable stability of a LAC. (It should be noted that in contrast to our procedure in E272, in order to conserve our very limited E629 running time, we elected not to carry out a direct calibration of the LAC using electrons.) When corrected for acceptance and the $\eta \rightarrow \gamma\gamma$ branching ratio, we obtain an η/π^0 production ratio of $.48 \pm .03$ for $p_T > 2$ GeV/c. This is in excellent agreement with the value previously obtained by the BNL-CIT-LBL collaboration in

the M2 beam. (The earlier measurement was made using a hydrogen target; the present measurement is for a carbon target.)

Besides π^o and η mesons, the other uninteresting potential sources of high p_T single photons are η' and ω mesons. In both cases, there is a strong suppression due to a low branching ratio for decays into the relevant channel: the decay $\eta' \to \gamma\gamma$ is suppressed by a factor of 20 relative to the decay $\eta \to \gamma\gamma$, and the decay $\omega \to \pi^o\gamma$ has a branching fraction of only 8.8%. For $\omega \to \pi^o\gamma$, the kinematics is in addition unfavorable to the production of a single γ at high p_T. For these reasons, the contamination of our experimental sample of single γ's from these sources is negligible. However, we do see a small, but statistically significant, ω signal in our 3γ events. This can be seen in Fig. 5 in which we display the 3γ mass spectrum for increasingly restrictive cuts on p_T. The $\omega \to \pi^o\gamma$ events, which appear as only a small shoulder when the lower p_T data are included, form an increasingly more well-defined peak as the p_T threshold is raised; the statistical significance of the ω peak is $\sim 4\sigma$. (The enhancing effect of the p_T cut is partially the result of the increased acceptance of our apparatus for higher p_T and, therefore, in general, higher energy ω's.) Due to our diminished acceptance (assuming an identical production distribution, our $\eta' \to \gamma\gamma$ acceptance is $\sim$40% of our acceptance for $\eta \to \gamma\gamma$), coupled with the intrinsic η' branching ratio, we only anticipate $\sim$14 η' events in a 80 MeV 2γ mass band centered on the η' mass (assuming identical "a priori" η and η' production rates). In light of our observed 2γ background of $\sim$16 events/20 MeV in this mass region, we are not statistically sensitive to an enhancement of this magnitude.

Finally, we display in Fig. 6 a comparison between our measured ratio of π^o inclusive production in p-Carbon and in π^+-Carbon collisions with the published results of G. Donaldson et al.[2] taken at the same energy

(the shaded region on the graph). This agreement, taken together with the preceding, gives us considerable confidence in the basic reliability of our data.

Turning therefore to our 1γ sample, we display in Fig. 7 the measured p_T spectrum for these events. The top histogram contains all of the data with only a hadron-eliminating cut applied (see below), while the lower histogram has had additional cuts applied which can be seen to remove the high p_T tail. The various cuts applied can be described as follows:

(a) Hadron Cut. The use of Pb plates provided a device having a thickness of 25 radiation lengths, but only 1.2 absorption lengths. This results in a very high level of discrimination against hadron induced showers. To be explicit, in Fig. 8 we display the fraction of pions which deposit more than a given percentage of their total energy in the LAC (these data are taken from E272). Less than 10% of all pions deposit in excess of 60% of their total energy in the LAC. (It should be noted that the apparent p_T of a shower is lowered by the same fraction as is its total energy.) In Fig. 9, we present the fractions of pions and electrons (equivalent to photons) which deposit less than a given percentage of their total deposited energy in the back half of the LAC; we have excluded the 30% of the pions which deposit less than 10% of their total energy. It should be noted that a E_{BACK}/E_{LAC} cut of <.2 will have the effect of eliminating 90% of the remaining pions at a cost of only 10% of the electrons. When considered in combination with the consequences of Fig. 8, it is clear that hadrons originating from the target give rise to a negligible level of high p_T background.

(b) Timing Cut. As previously indicated, the p_T trigger modules also permitted us to time the energy deposition in the LAC. In Fig. 10 we display this timing data as a function of the shower p_T. (The origin is relative to the time of arrival of a photon produced in the target.) As can be seen, at low p_T, there is a clean peak at the origin, with a σ of $\sim$6 nsec and relatively little background. As the p_T values increase, however, the in-time peak diminishes, and late arriving showers begin to enter, and eventually to dominate. (As a further indication of our timing resolution, note the "bucket structure" of the data in Fig. 10(c).) We can understand the data shown in Fig. 10 as follows. Our veto circuitry effectively protected us against both early accidentals and late accidentals occurring within 50 nsec of the event. (By accidental, we mean energy deposition in the LAC, from a source other than particles from our target, which is in random coincidence with an interaction in the target.) We were not able to protect against accidentals arriving later than 50 nsec after the prompt time due to the limited delay in our version of the LAC amplifiers; the most recent version of these amplifiers has twice as much internal delay. The efficacy of a time cut, centered at the prompt time, in removing high p_T background is obvious from the data shown, and this is one of the two cuts applied in Fig. 7.

(c) Directionality Cut. The origin of the accidentals can be further analyzed through an examination of their angle of arrival at the LAC. This angle can be measured by the analysis schematically described in Fig. 11. Due to the close proximity of the LAC to the target, photons

originating in the target arrive at the LAC at angles which are significantly different from what would be the case if they were entering parallel to the beam line. Due to the excellent spatial resolution of the LAC, a comparison of the shower location in the front and back of the detector permits us to determine the entrance angle of each shower. In Fig. 12 we display a scatterplot of the experimental data in which we show the correlation between the X position of the shower in the front half of the LAC, and the difference between its observed and predicted position in the back half, based on the assumption that the shower arose from a photon originating in the target; the geometry is as described in Fig. 11. Photons originating in the target show up in Fig. 12 as a (vertical) band at zero; the second (angled) band is precisely what would be expected from tracks entering the LAC parallel to the beam line.[3] (The horizontal gaps in the scatterplot arise from a few back strips in the LAC which had broken cables inside the detector.) The second cut applied to the data shown in Fig. 7 is the requirement that the observed shower position in the back half of the LAC agree with that expected for a target-originating photon.

The explanation of the accidentals as arising from showers produced by particles in the beam "halo" (we are not referring to the normal halo immediately outside the beam proper, but to particles approximately a meter off the beam axis) also explains their tendency to show up primarily at high p_T, since by attributing them to the target we are systematically overestimating their angular divergence from the beam axis. It is not clear whether these halo particles are hadrons or possibly photons originating from interactions in the downstream face of our hielding. In addition to our target cave, we employed a considerable

amount of upstream shielding; clearly more was needed, and we will certainly employ far more shielding in E695. (The amount of shielding we used was limited by what we could obtain and get rigged into position in time for the execution of E629.) It should also be noted that the accidental problem might have been far more severe if the hadron rejection capability of our LAC were not extremely high. (Our E629 accidental triggers were presumably due to hadrons, even though the interactions of these hadrons in the LAC were highly atypical.)

Having thus obtained a clean sample of high p_T single photons, we next need to determine what fraction of these arise from π^o's and η's. For this determination, we made use of the π^o and η events from our 2γ sample (see Fig. 4). For every observed event we generated a sample of events having the same y_{cm} and p_T values, but randomly distributed in production azimuth and in decay angles. A variable number of events were generated for each observed event in such a way that each input event contributed equally to the 2γ generated sample. This procedure has the effect of weighting each observed event according to its acceptance. To account for the γ detection efficiency (both hardware and software), every accepted γ was required to have an energy in excess of 1.2 GeV. A detailed analysis of background noise in the LAC, and of the LAC reconstruction program efficiency, indicates that this is a very conservative cut, and that photon losses above this energy are indeed negligible. To account for the variation of the effective p_T threshold across the detector (see our earlier discussion), a model of the trigger was developed which reproduced the data shown in Fig. 2. Only those

generated events which would have triggered the apparatus were then accepted. We have investigated the effect of including the trigger efficiency in the Monte Carlo, and have verified that it only influences the predicted γ/π^o ratio at our lowest p_T values ($\sim$2 GeV/c). Ignoring the trigger efficiency in this region results in an overestimation of the predicted γ background (by ~5%).

A very stringent test of the validity of the Monte Carlo model lies in its ability to reproduce the observed 2γ energy asymmetry distribution for π^o and η^o decays. These distributions, which would be flat in the absence of background and experimental losses, are highly sensitive to such effects.

In Fig. 13 we display the background-subtracted π^o and η asymmetry distributions (Figs. 13(b) and 13(d), respectively) along with the asymmetry contributions attributed to the background events (Figs. 13(a) and 13(c). Since the background arises from essentially uncorrelated γ's, it is seen to have a very different shape from that characterizing π^o and η decays. The number of events in the background were determined from Fig. 4. The shape of the asymmetry distribution arising from the background events was determined as follows. Using five mass intervals which excluded the π^o and η mass bands, the variation of the average background asymmetry with mass was determined, and used to predict the average background asymmetry in the π^o and η mass regions. Asymmetry data from below and above the π^o and η mass bands were then linearly combined so as to yield the predicted average asymmetry within these bands. These combined data were then normalized to the number of background events predicted by Fig. 4 and the resulting distributions are plotted in Figs. 13(a) and (13(c), and are subtracted in Figs. 13 (b) and 13(d)[4].

The curves shown in Figs. 13(b) and (d) are the predictions of the Monte Carlo which are seen to be in excellent agreement with the data. Based on this level of agreement, we can with confidence use the model to predict how many of the single γ's in our data sample arise from π^o and η decays. We wish to stress that these background γ's are precisely the ones that are missing in Figs. 13(b) and 13(d), and thereby produce the deviation from isotropy seen in the decay distributions. It also should be noted that the fiducial volume for accepting single γ's was smaller than that for accepting π^o's or η's.

Having thus determined the contribution to the single γ sample from π^o and η decays[5], we display in Fig. 14 the observed γ/π^o ratio for our selected class of events, along with the curve representing the expected background from π^o and η events (η decays yield $\sim$1/4 of the total estimated background). Both the π^o and η data have been corrected for the acceptance of the apparatus (both geometric and trigger effects). In Fig. 15 we display the background-subtracted γ/π^o ratio. The net ratio is clearly substantial. It is however important to keep in mind that the cuts which we have imposed on our data samples most probably serve to depress the π^o yield, and hence to enhance the value of the quoted ratio. It is for this reason not possible for us at this stage in our analysis to directly compare our experimental result to any other. What is, however, clear is that we were able to isolate in E629, despite the many experimental constraints imposed upon us, a sample of high p_T direct

photon events. In light of the underlying similarity between E629 and P695, this success represents perhaps the most significant evidence as to the basic soundness of our proposed experimental design.

(4) Most of the data acquired during E629 had more than two photons in the LAC. In Fig. 16 we show the γ-multiplicity distribution; the average number of reconstructed photons is 4.4. (The 0γ events are those which we believe to have been triggered by hadrons.) We have concentrated mostly on the 1γ and 2γ samples in preparing this appendix. However, we are able to detect clear signals in the higher multiplicity data. For example, in Fig. 17 we show the $\gamma\gamma$ mass distribution for the 3γ sample, for 2γ combinations with $p_T > 2.5$ GeV/c. Clear peaks at the π^o and η^o masses are apparent. In Fig. 18 we show the 2γ mass distribution for the 4γ, and in Fig. 19 for the $>4\gamma$ events (also with a $p_T > 2.5$ GeV/c cut); we see that relatively clean π^o peaks are present in all the data, but there is no η^o signal in the $>4\gamma$ events. These distributions encourage us to believe that we can, indeed, successfully handle high multiplicities in the LAC, and that a fully inclusive measurement of high p_T π^o and η^o production using our data should be relatively straight-forward.

(5) We have discussed the most important of these "surprises" in the context of the previous 4 items: the importance of protecting against coherent noise, the role played by the ballast capacitors, and the effect of even a small punch-through of hadrons in the beam halo. All of these effects were to some extent anticipated; nevertheless, in terms of their influence on our design of E695, our greater appreciation of their importance represents one of the principal benefits of E629.

In conclusion, we believe that E629 was completely successful in its goal of guiding us in our design of P695. Indeed, in many respects it exceeded its mandate, and became a direct photon measurement in itself.

Footnotes and references

1. The original Fermilab LAC amplifiers were the result of a collaborative effort between Rochester and Fermilab. (See T. Droege, F. Lobkowicz, and Y. Fukushima, IEEE Transactions on Nuclear Science, NS-25 1, 687 (1978)), and were used in E272, and subsequently in E629. The basic design was then improved upon by T. Droege, and this is the version currently in use by E515 (and others).
2. G. Donaldson, et al., Phys. Rev. Letts. 36, 1110 (1976).
3. We have examined the correlation between the timing and angle cuts, and have verified that they are highly correlated as expected. We also took some data replacing the interaction requirement by a random strobe of the same frequency, and verified that accidentals occurred at the rate anticipated from an analysis based on Figs. 10 through 12; we also found that the time and angle correlation for these accidentals was the same as that observed in the background to the normal data.
4. We have investigated the efficacy of the procedure described via a Monte Carlo analysis of uncorrelated photons, and found it to be a very reasonable means of predicting the background contribution to the π^o and η asymmetry distributions.
5. In order to verify the validity of our analysis technique, we also carried out a separate Monte Carlo analysis in which we generated π^o and η events according to the previously measured differential cross section of G. Donaldson, et al., Phys. Letts. 73B, 375 (1978). We then analyzed these events according to the techniques outlined

in this appendix, and determined thereby that we correctly predicted the number of single photons produced by π^o and η sources.

Figure Captions.

Figure 1: The layout for E629. The distance from the target to the LAC is approximately 8 meters.

Figure 2: Trigger efficiency for π^o detection in right-hand side of the LAC.

Figure 3: Trigger efficiency for single photon detection in right-hand side of the LAC.

Figure 4: The two-photon mass spectrum in the π^o and η region. The curves show the assumed background.

Figure 5: The three-photon mass spectrum for a range of p_T cuts.

Figure 6: The ratio of inclusive π^o production at large p_T by protons and pions on Carbon.

Figure 7: The p_T distribution of single showers, with only the hadron cut and with hadron, direction and timing cuts applied.

Figure 8: The fraction of charged pions depositing more than a given percentage of their total energy E_{HAD} in the LAC.

Figure 9: The fraction of pions and electrons which deposit less than a given percentage of the total deposited energy in the back half of the LAC.

Figure 10: Histograms of the distribution of the arrival times of single photons in the LAC. Most hadrons have already been eliminated by a (E_{BACK}/E_{LAC}) cut. The shaded histograms show showers which survive the directionality cut.

Figure 11: The definition of ΔX_B used for the directionality cut. Note that $\Delta X_B = 0$ corresponds to showers originating in the target.

Figure 12: Scatterplot of the directionality parameter ΔX_B against the position in the LAC (for single photons). The two horizontal gaps in the scatterplot correspond to isolated dead channels in the back section of the LAC.

Figure 13: Decay asymmetry distributions in the π^o and η mass region. For details of the background determination and subtraction consult the main text.

Figure 14: Ratio of isolated single photons to isolated π^o mesons. The curve shows the expected background due to π^o and η events.

Figure 15: Same as Figure 14, but with the background subtracted.

Figure 16: Multiplicity distribution of photons after removal of all hadronic showers.

Figure 17: The two-photon mass distribution for three-photon events. Only those $\gamma\gamma$ combinations are plotted whose p_T is greater than 2.5 GeV/c.

Figure 18: The two-photon mass distribution for four-photon events. The p_T of each $\gamma\gamma$ pair plotted is required to be >2.5 GeV/c.

Figure 19: Same as Figure 18, for all events with a photon multiplicity greater than four.

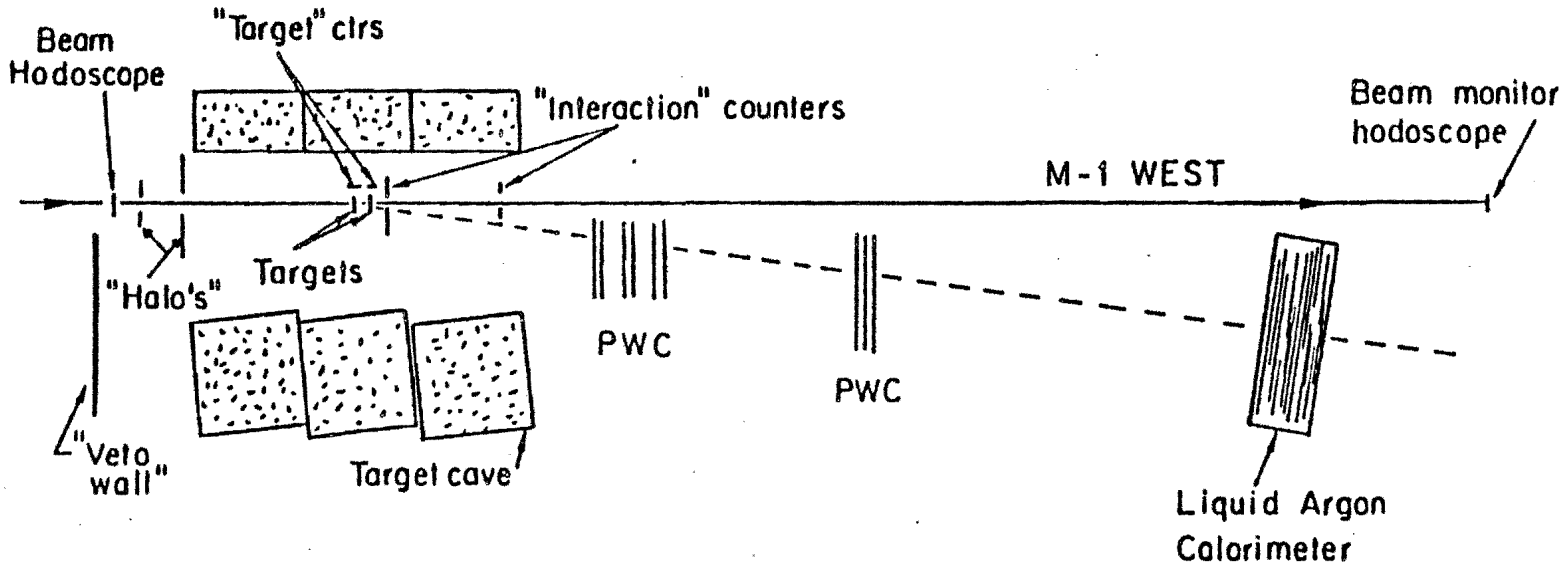
Beam
Hodoscope
"Target" ctrs
"Interaction" counters
Beam monitor
hodoscope
M-1 WEST
"Halo's"
Targets
PWC
PWC
"Veto
wall"
Target cave
Liquid Argon
Calorimeter

Fig. 1

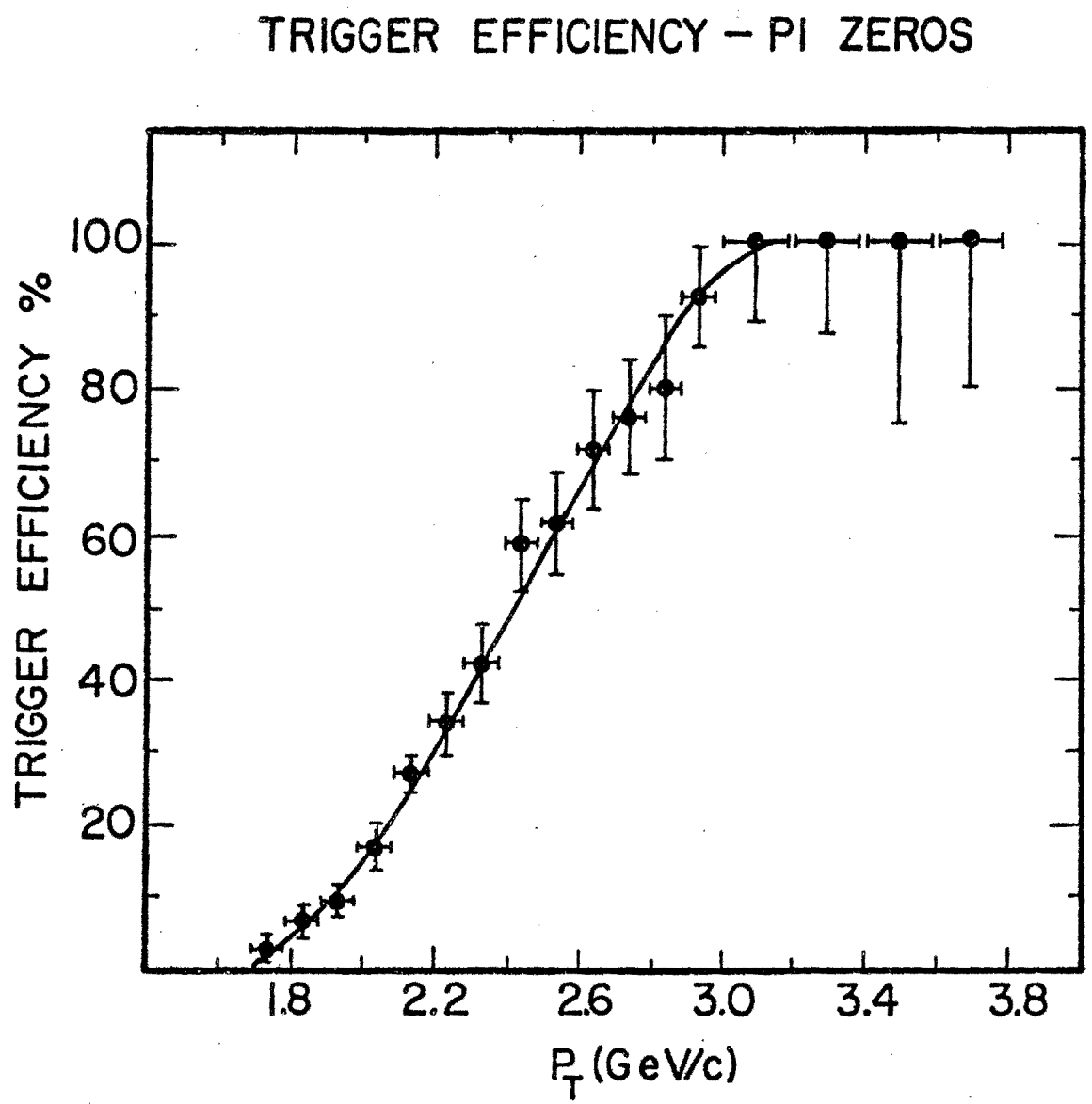
TRIGGER EFFICIENCY – PI ZEROS
TRIGGER EFFICIENCY %
100
80
60
40
20
1.8
2.2
2.6
3.0
3.4
3.8
P_T (GeV/c)

Fig. 2

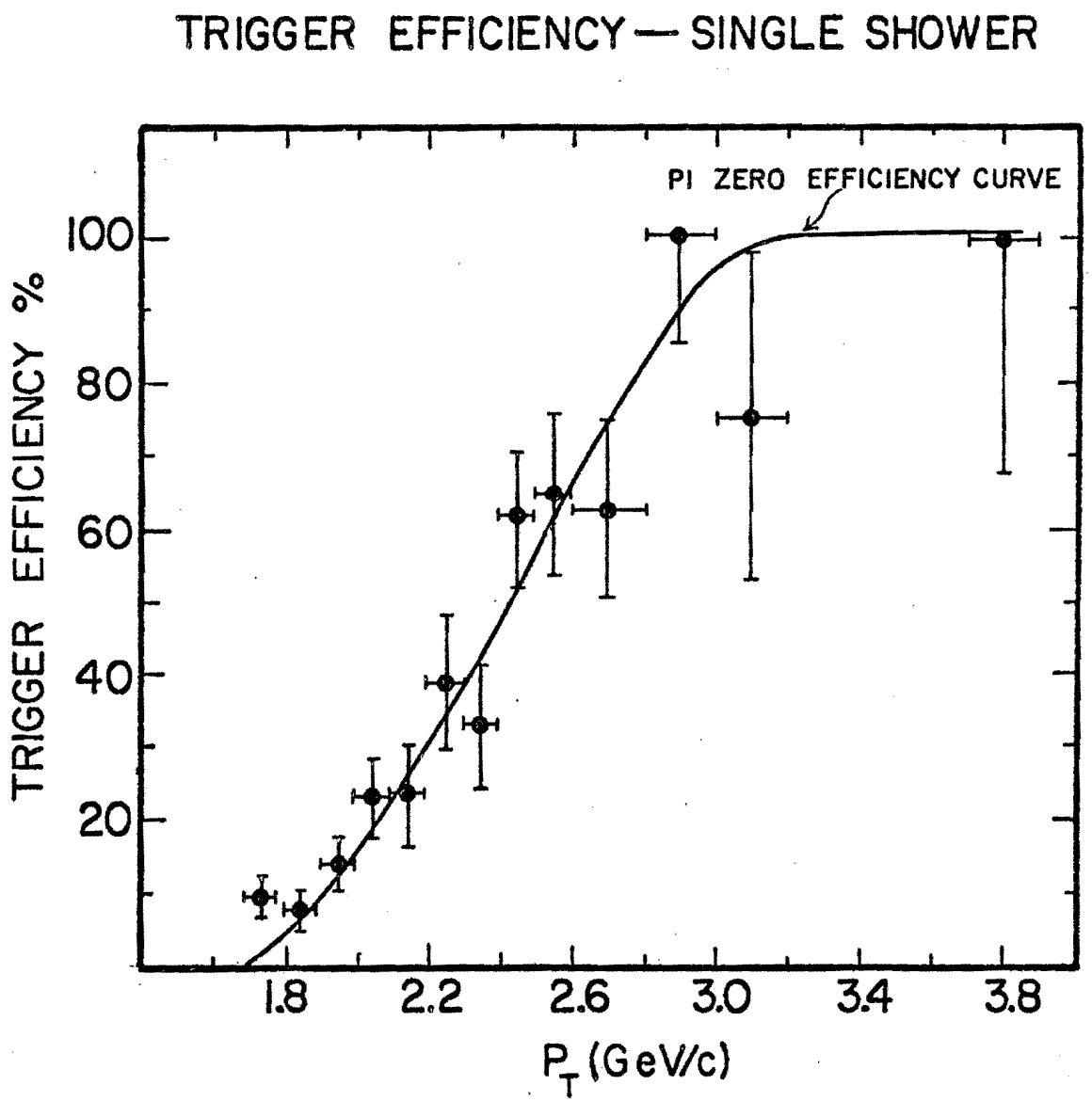
TRIGGER EFFICIENCY — SINGLE SHOWER
PI ZERO EFFICIENCY CURVE
TRIGGER EFFICIENCY %
100
80
60
40
20
1.8
2.2
2.6
3.0
3.4
3.8
P_T (GeV/c)

Fig. 3

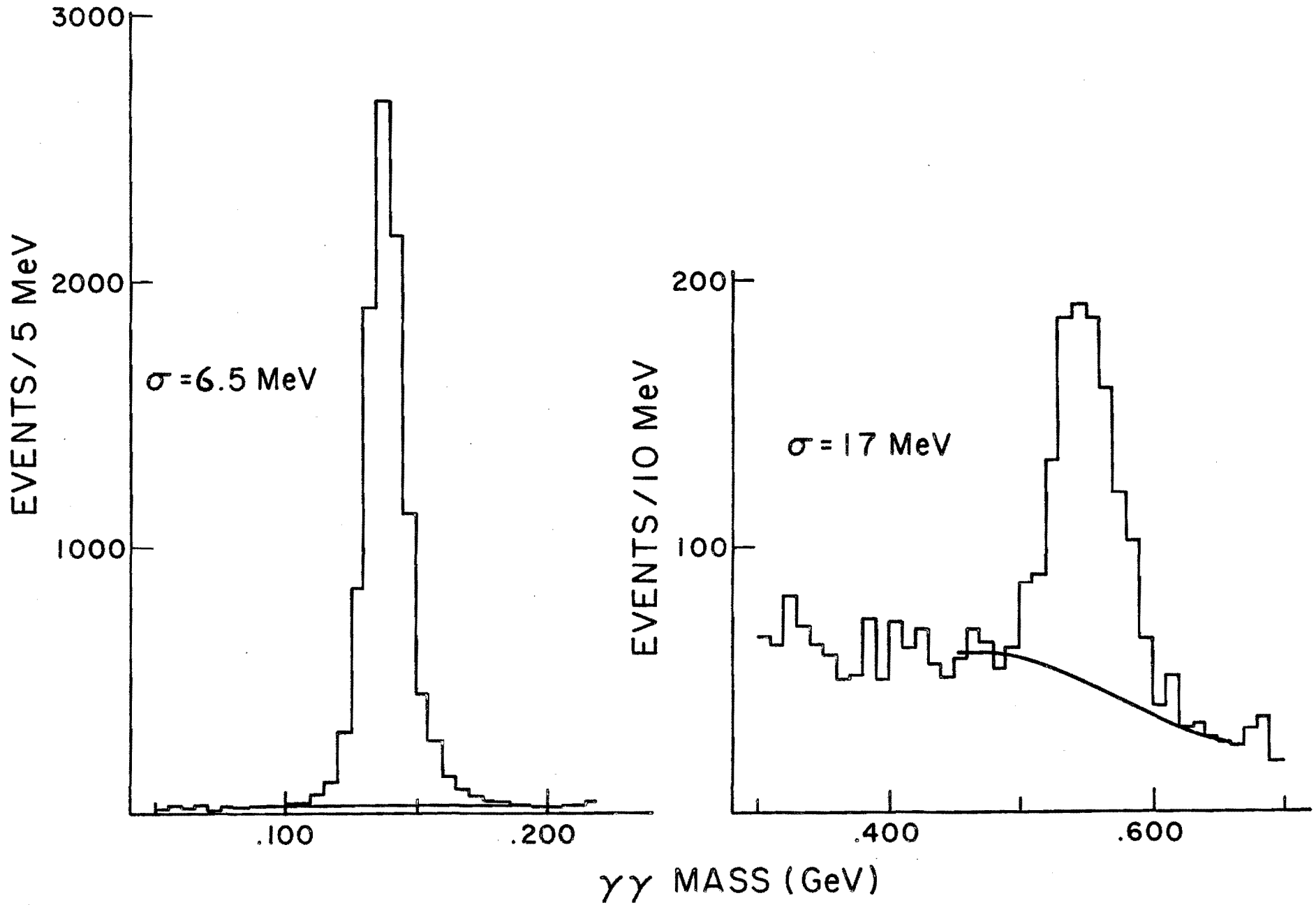
3000
2000
1000
EVENTS / 5 MeV
σ = 6.5 MeV
.100
.200
200
100
EVENTS / 10 MeV
σ = 17 MeV
.400
.600
γγ MASS (GeV)

Fig. 4

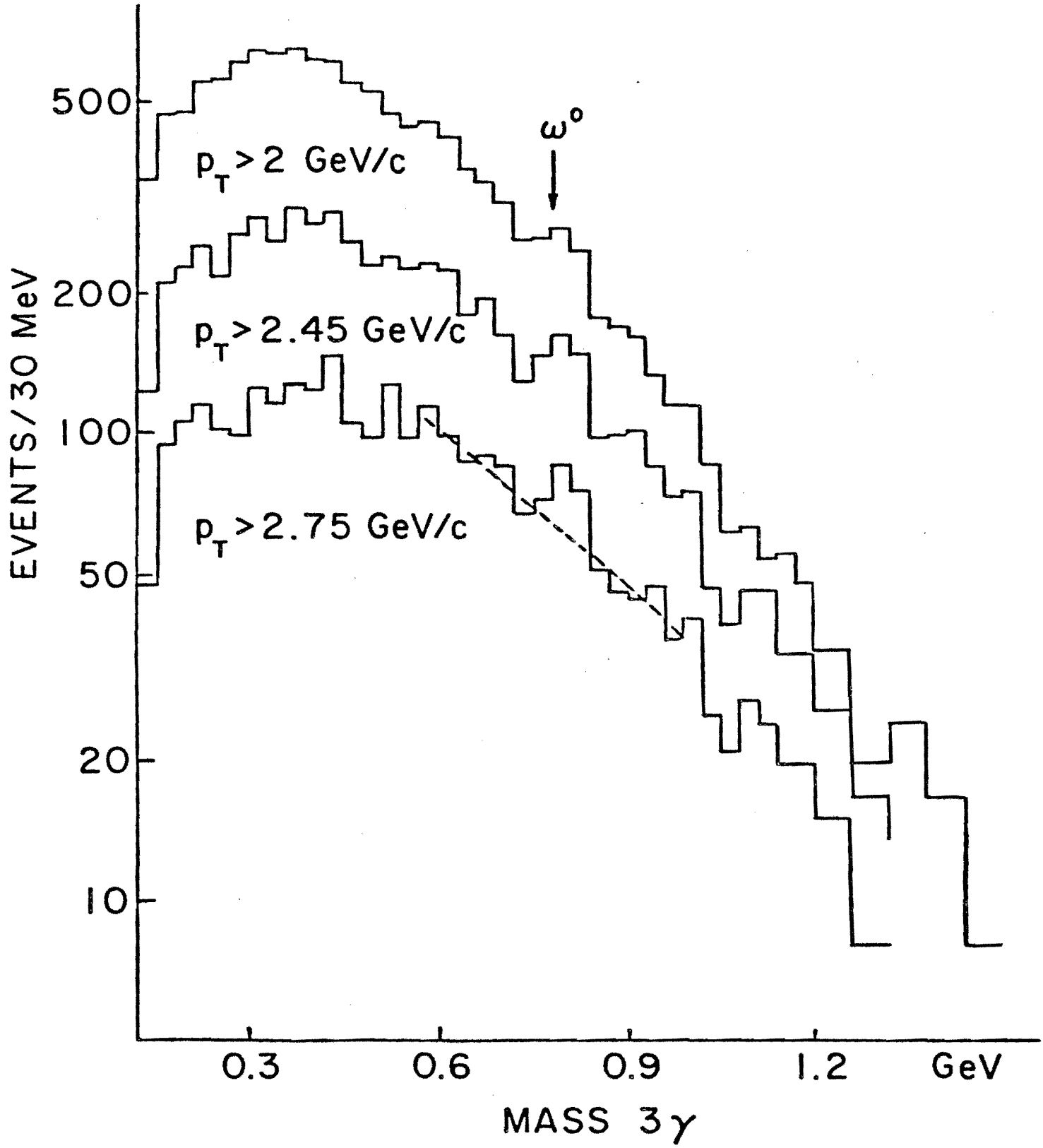
500
200
100
50
20
10
EVENTS/30 MeV
$p_T > 2$ GeV/c
$p_T > 2.45$ GeV/c
$p_T > 2.75$ GeV/c
ω^0
0.3
0.6
0.9
1.2
GeV
MASS 3γ

Fig. 5

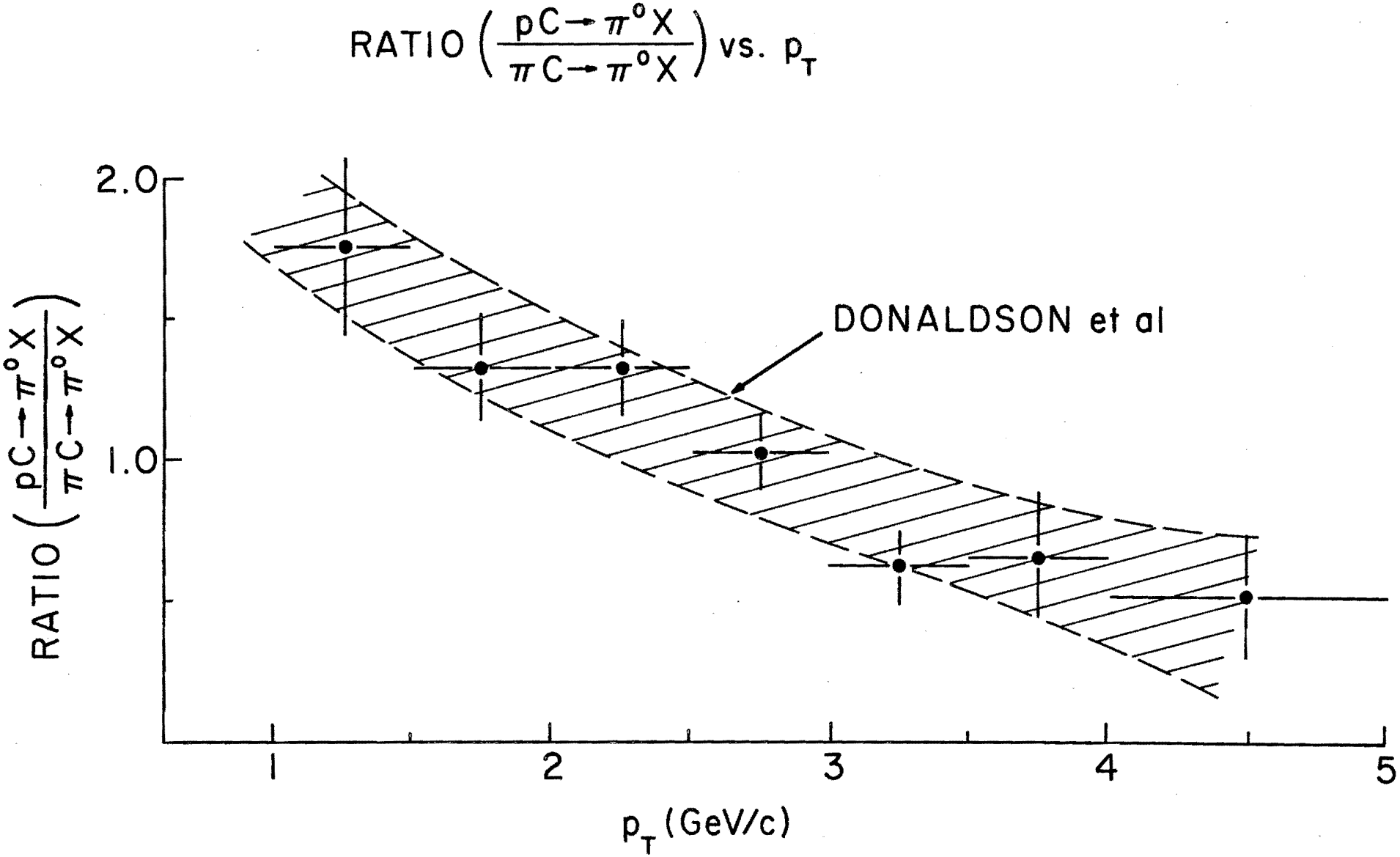
RATIO $\left(\frac{pC \to \pi^0 X}{\pi C \to \pi^0 X}\right)$ vs. p_T
2.0
1.0
RATIO $\left(\frac{pC \to \pi^0 X}{\pi C \to \pi^0 X}\right)$
DONALDSON et al
1
2
3
4
5
p_T (GeV/c)

Fig. 6

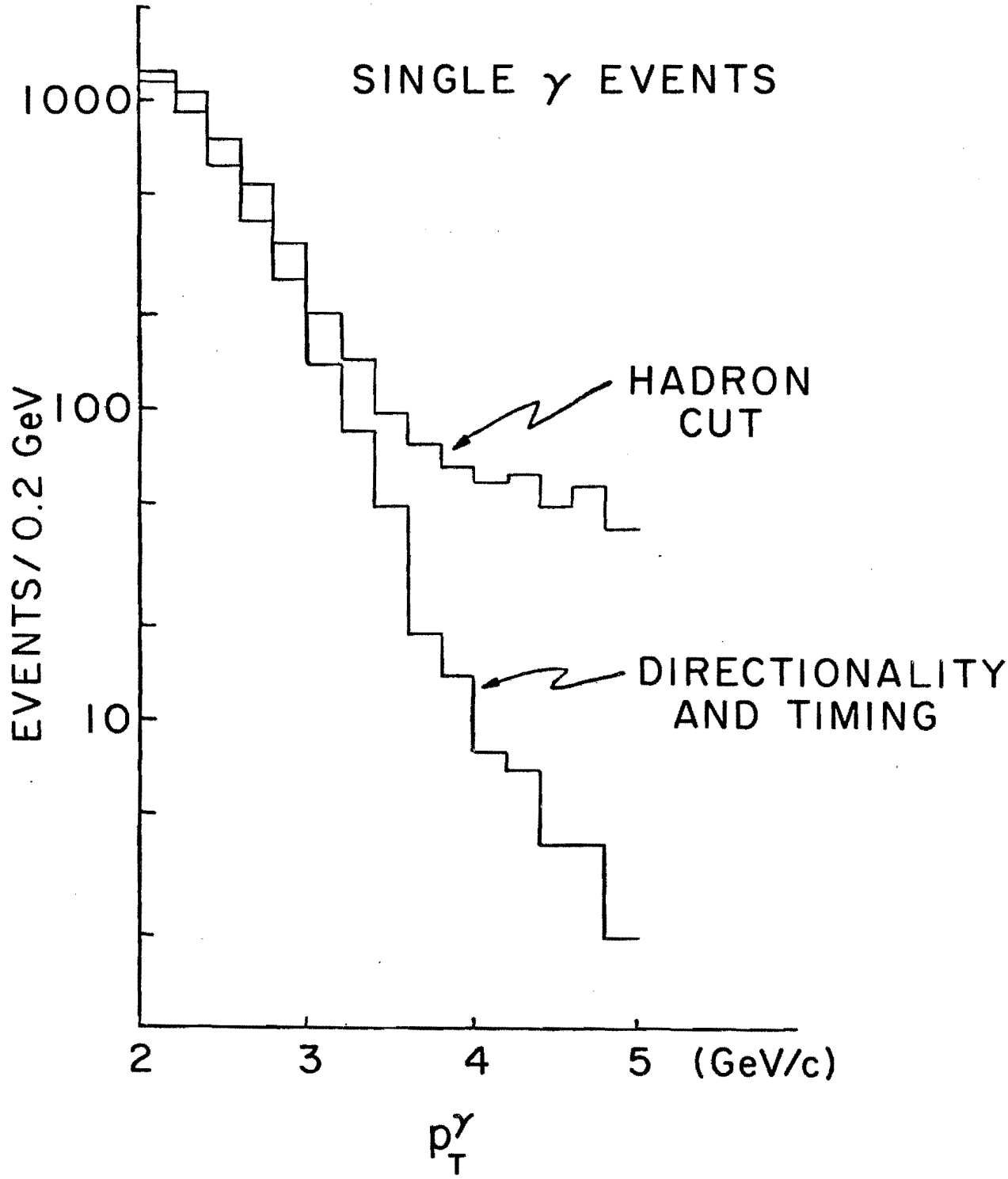
SINGLE γ EVENTS
1000
100
10
EVENTS/ 0.2 GeV
HADRON
CUT
DIRECTIONALITY
AND TIMING
2
3
4
5
(GeV/c)
p_T^γ

Fig. 7

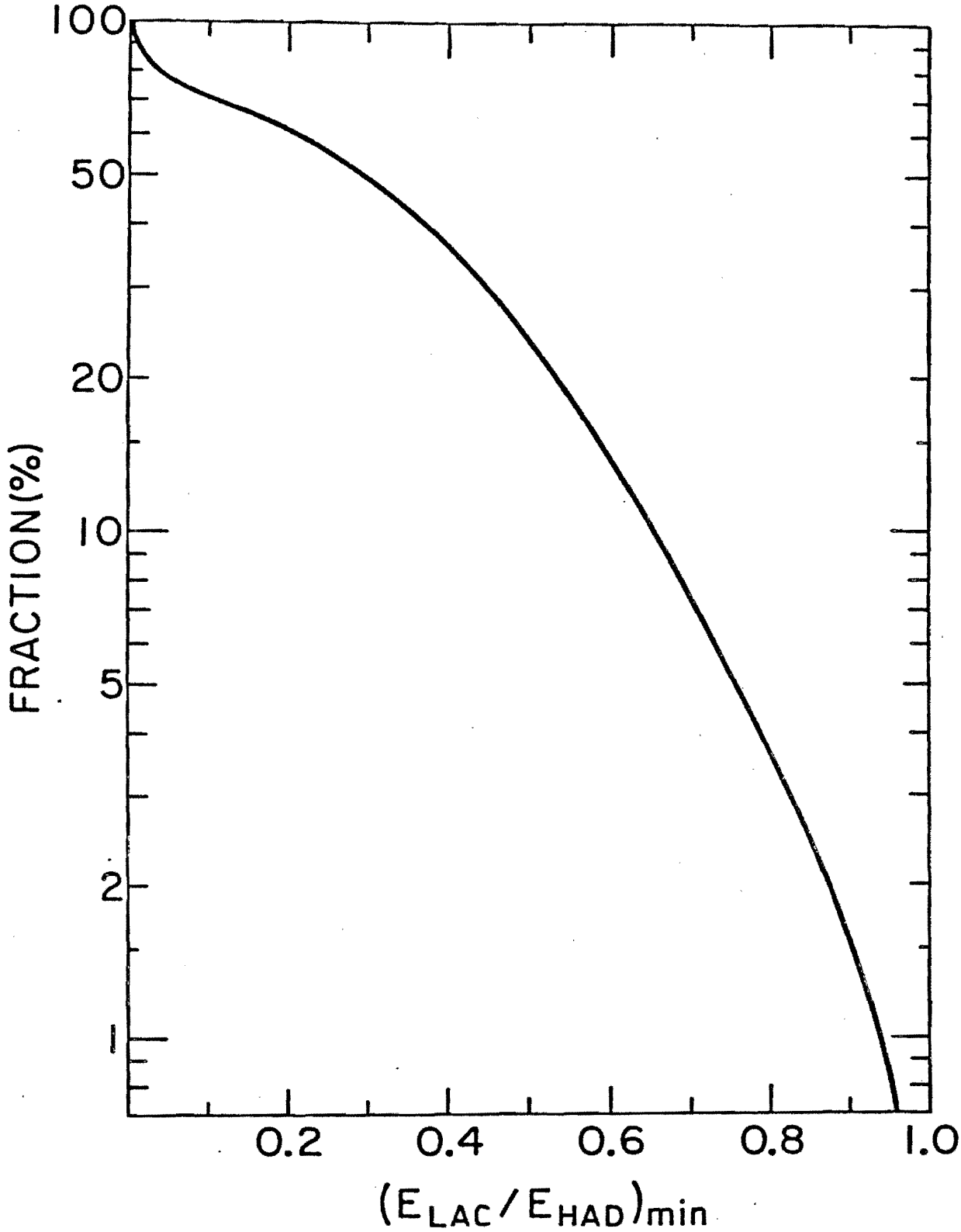

Fig. 8

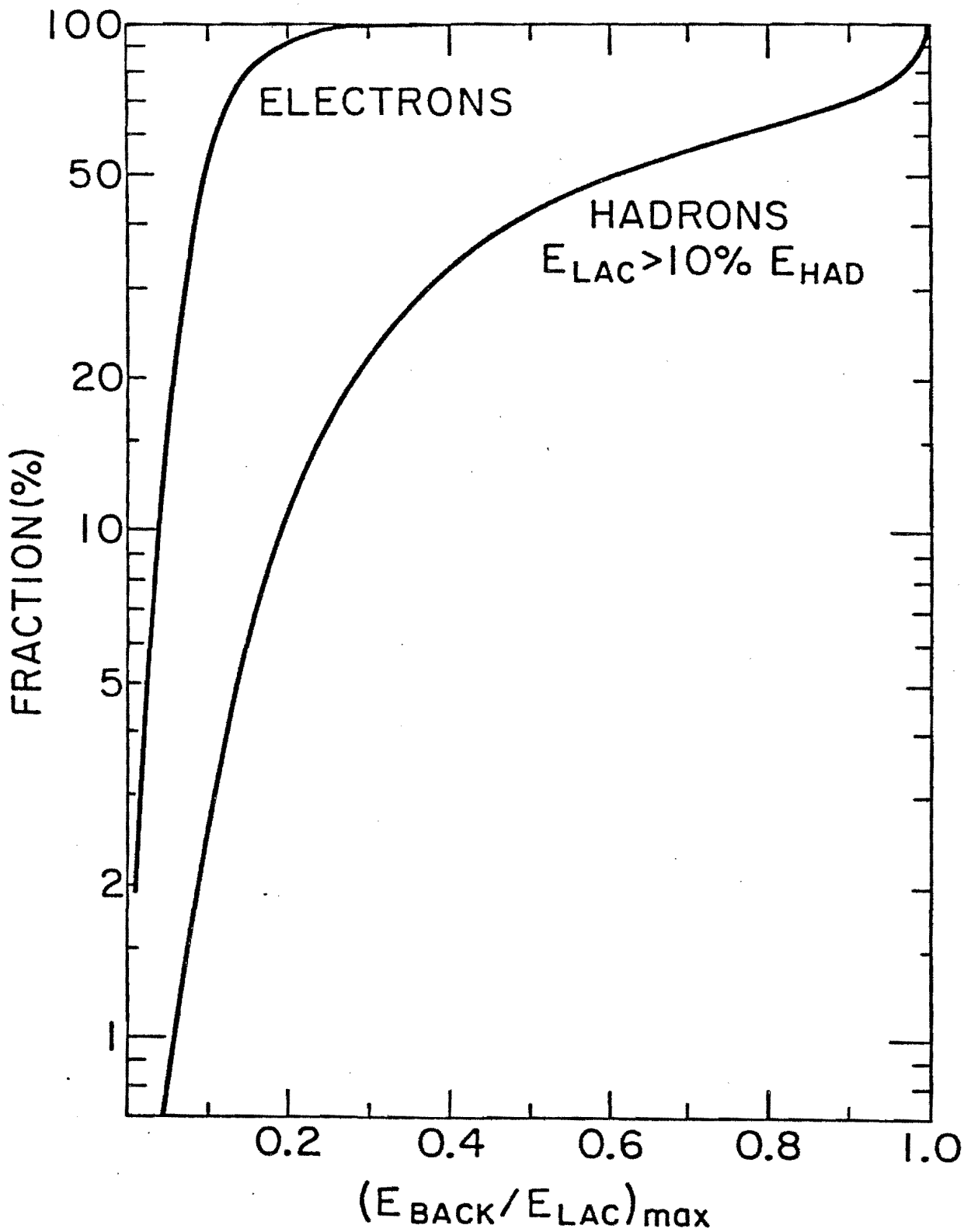
100
50
20
10
5
2
1
FRACTION(%)
ELECTRONS
HADRONS
E_{LAC}>10% E_{HAD}
0.2
0.4
0.6
0.8
1.0
$(E_{BACK}/E_{LAC})_{max}$

Fig. 9

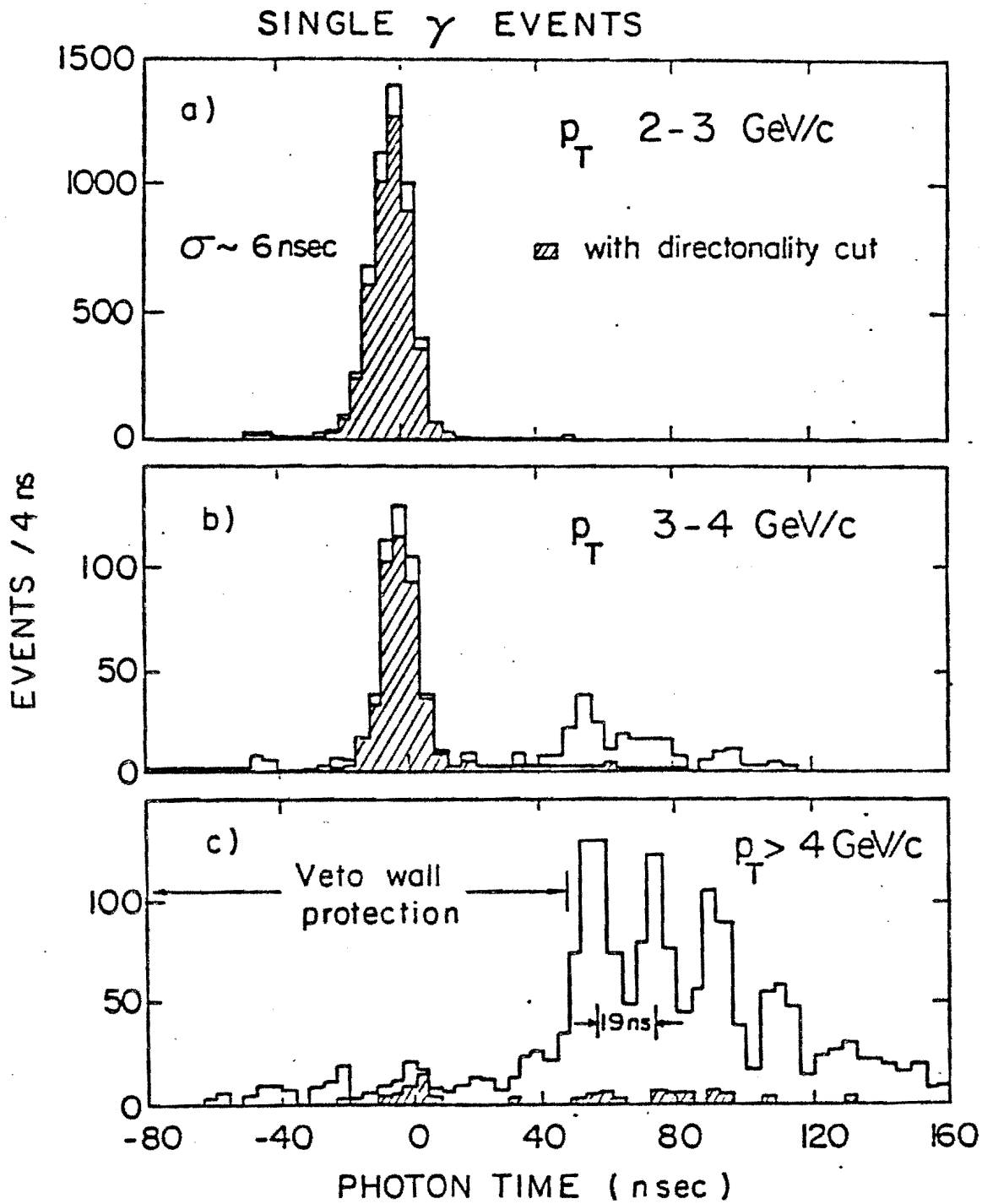
SINGLE γ EVENTS
a)
p_T 2-3 GeV/c
σ~ 6 nsec
with directonality cut
b)
p_T 3-4 GeV/c
c)
p_T> 4 GeV/c
Veto wall protection
19ns
EVENTS /4 ns
PHOTON TIME (nsec)
1500
1000
500
0
100
50
-80
-40
40
80
120
160

Fig. 10

$$\Delta X_B = \frac{T_{LAC}}{D_{LAC}} (X_F - X_0)$$

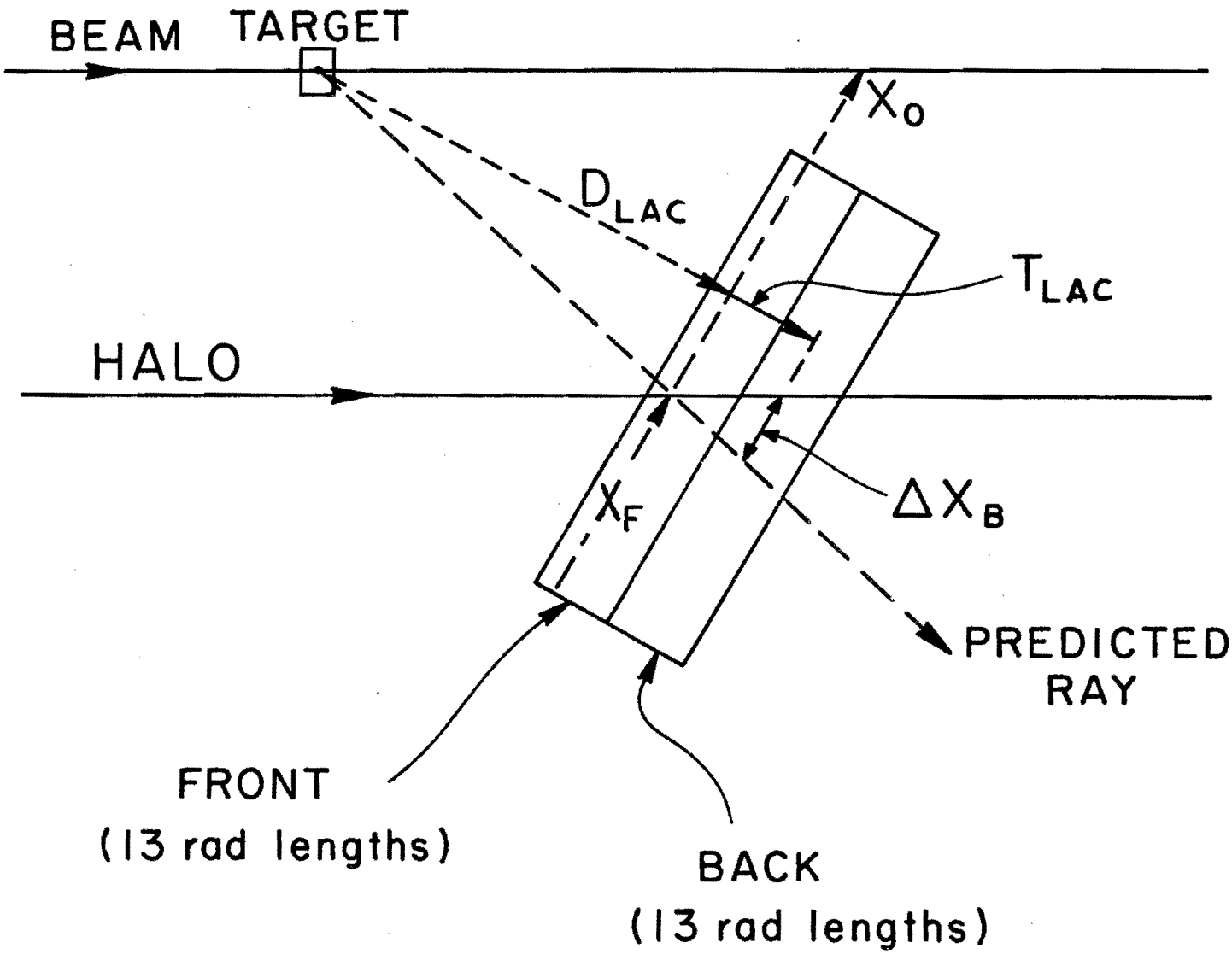

Fig. 11

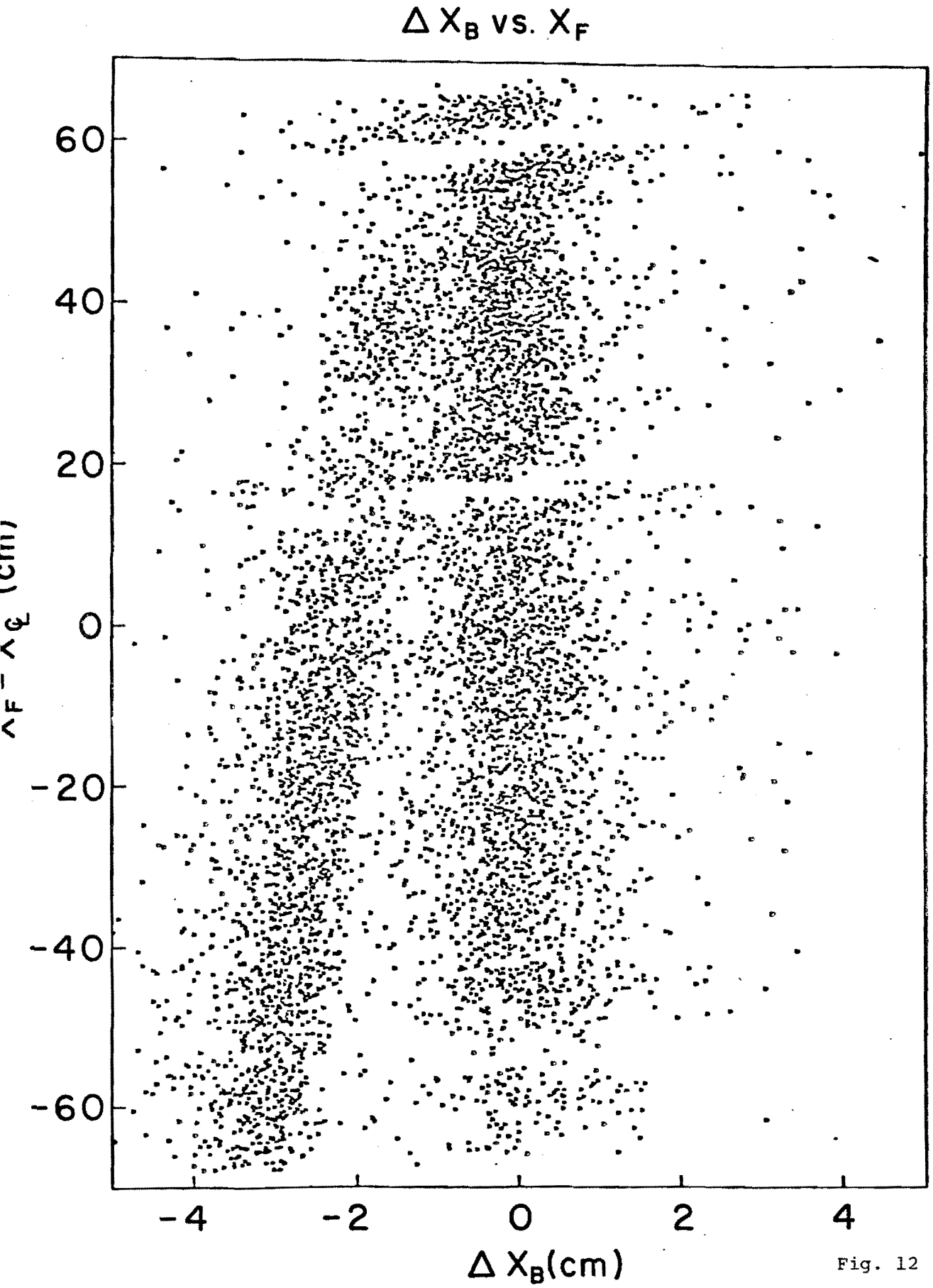

Fig. 12

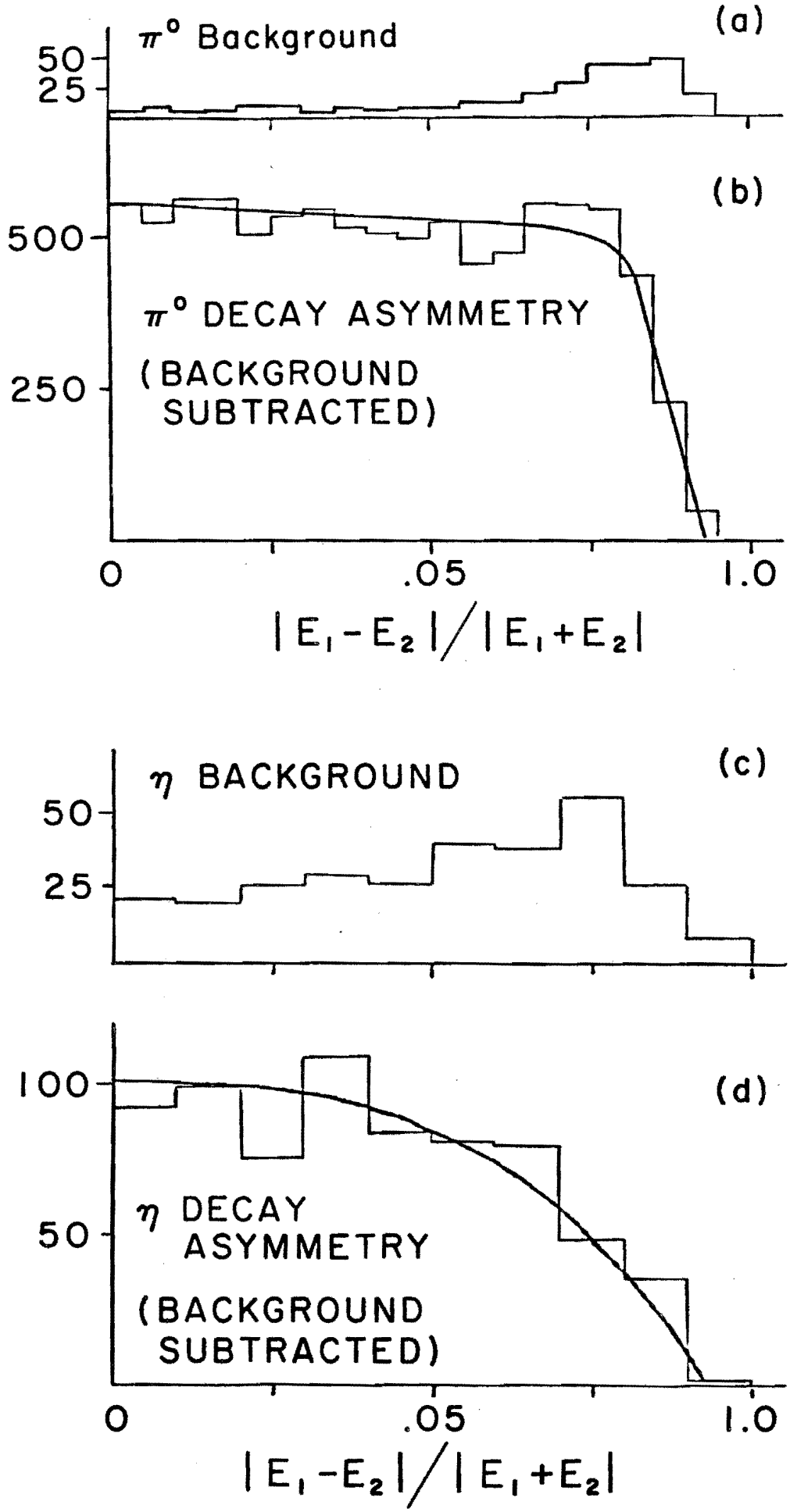
(a)
π° Background
50
25
(b)
500
250
π° DECAY ASYMMETRY
(BACKGROUND SUBTRACTED)
0
.05
1.0
|E₁-E₂|/|E₁+E₂|
(c)
η BACKGROUND
50
25
(d)
100
50
η DECAY ASYMMETRY
(BACKGROUND SUBTRACTED)
0
.05
1.0
|E₁-E₂|/|E₁+E₂|

Fig. 13

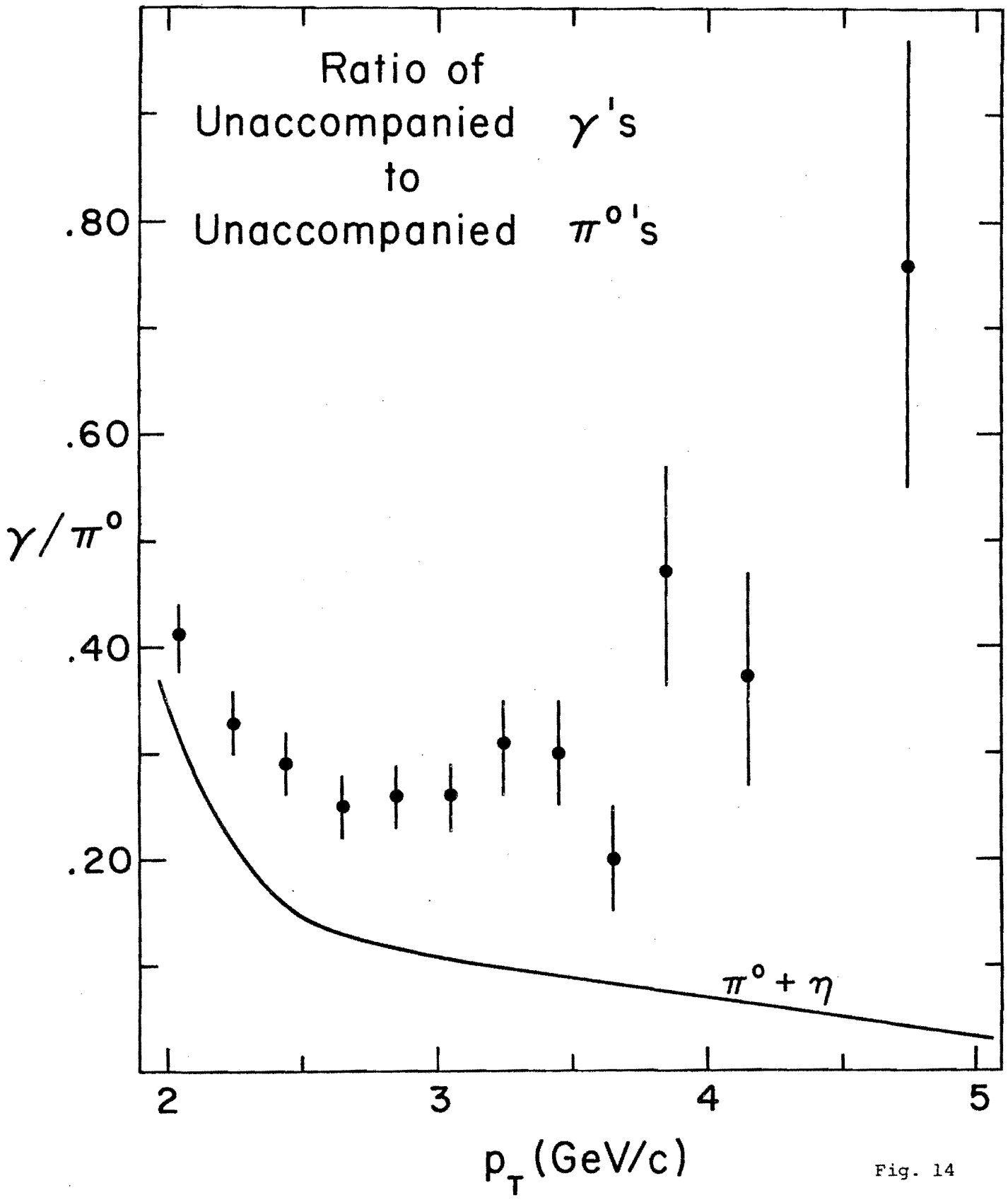
Ratio of
Unaccompanied γ's
to
Unaccompanied π°'s
.80
.60
.40
.20
γ/π°
π° + η
2
3
4
5
p_T (GeV/c)

Fig. 14

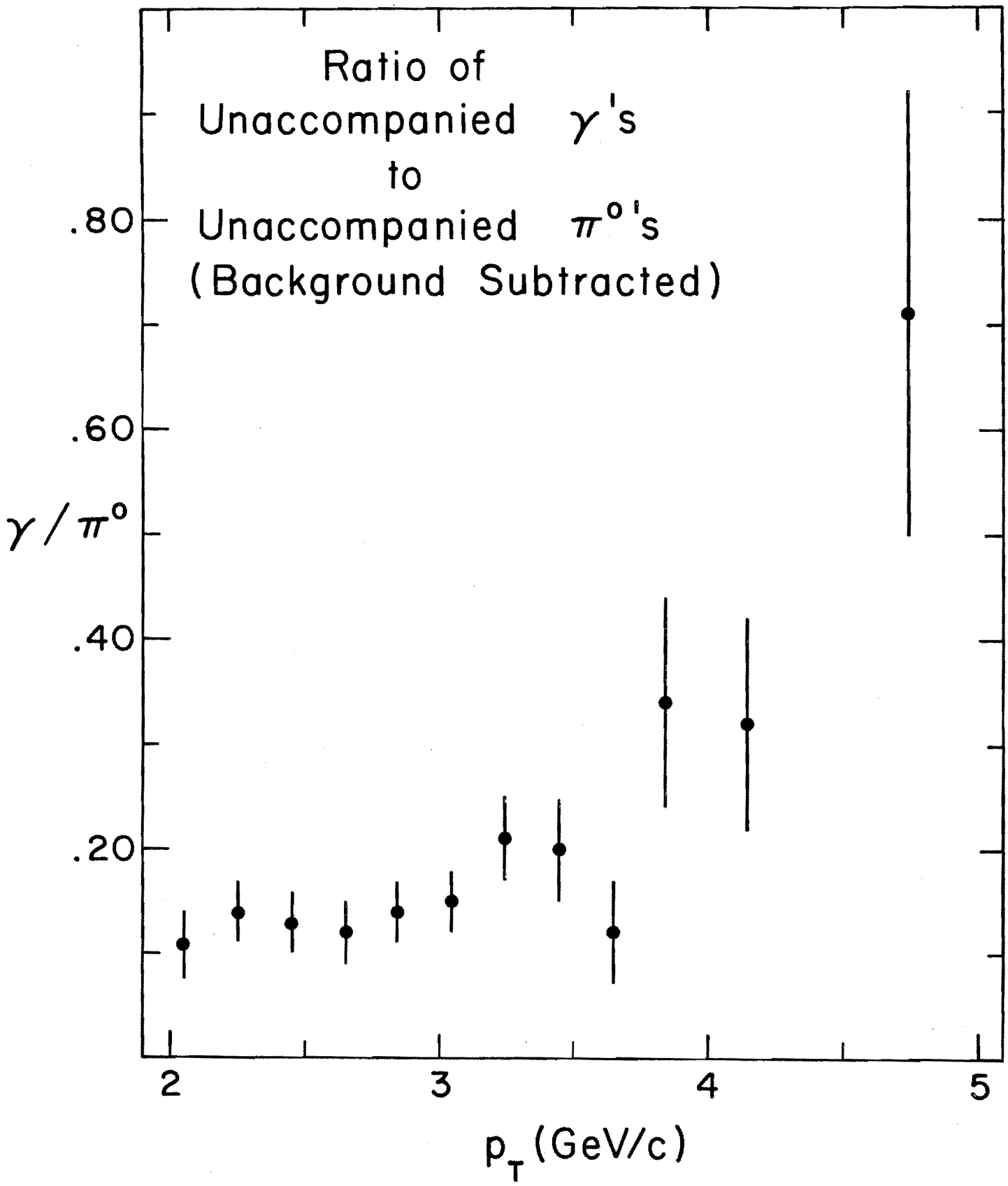
Ratio of
Unaccompanied γ's
to
Unaccompanied π°'s
(Background Subtracted)
.80
.60
.40
.20
γ / π°
2
3
4
5
p_T (GeV/c)

Fig. 15

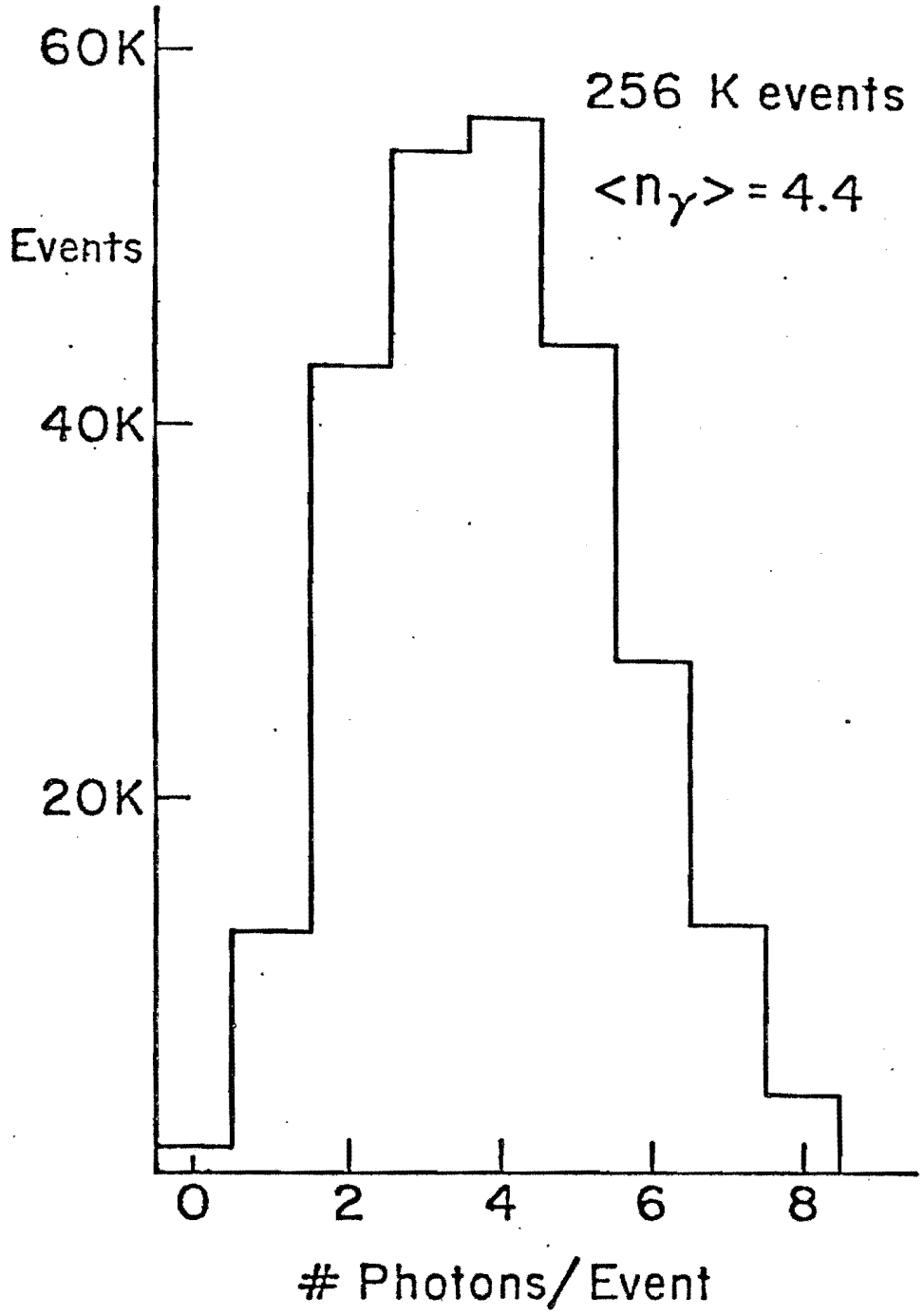
60K
40K
20K
Events
256 K events
$\langle n_\gamma \rangle = 4.4$
0
2
4
6
8
Photons/Event

Fig. 16

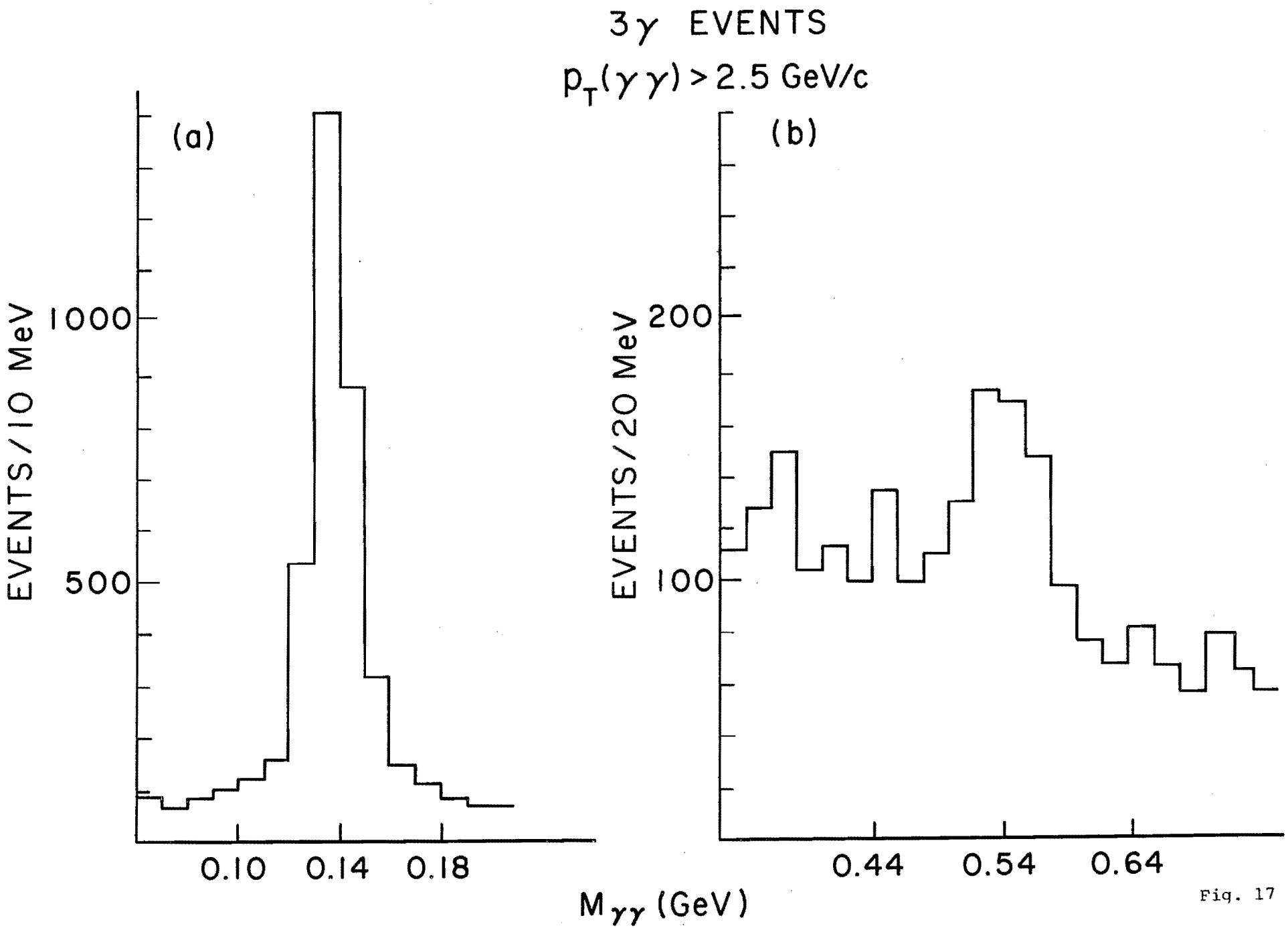
3γ EVENTS
$p_T(\gamma\gamma) > 2.5$ GeV/c
(a)
(b)
EVENTS/10 MeV
1000
500
EVENTS/20 MeV
200
100
0.10
0.14
0.18
0.44
0.54
0.64
$M_{\gamma\gamma}$ (GeV)

Fig. 17

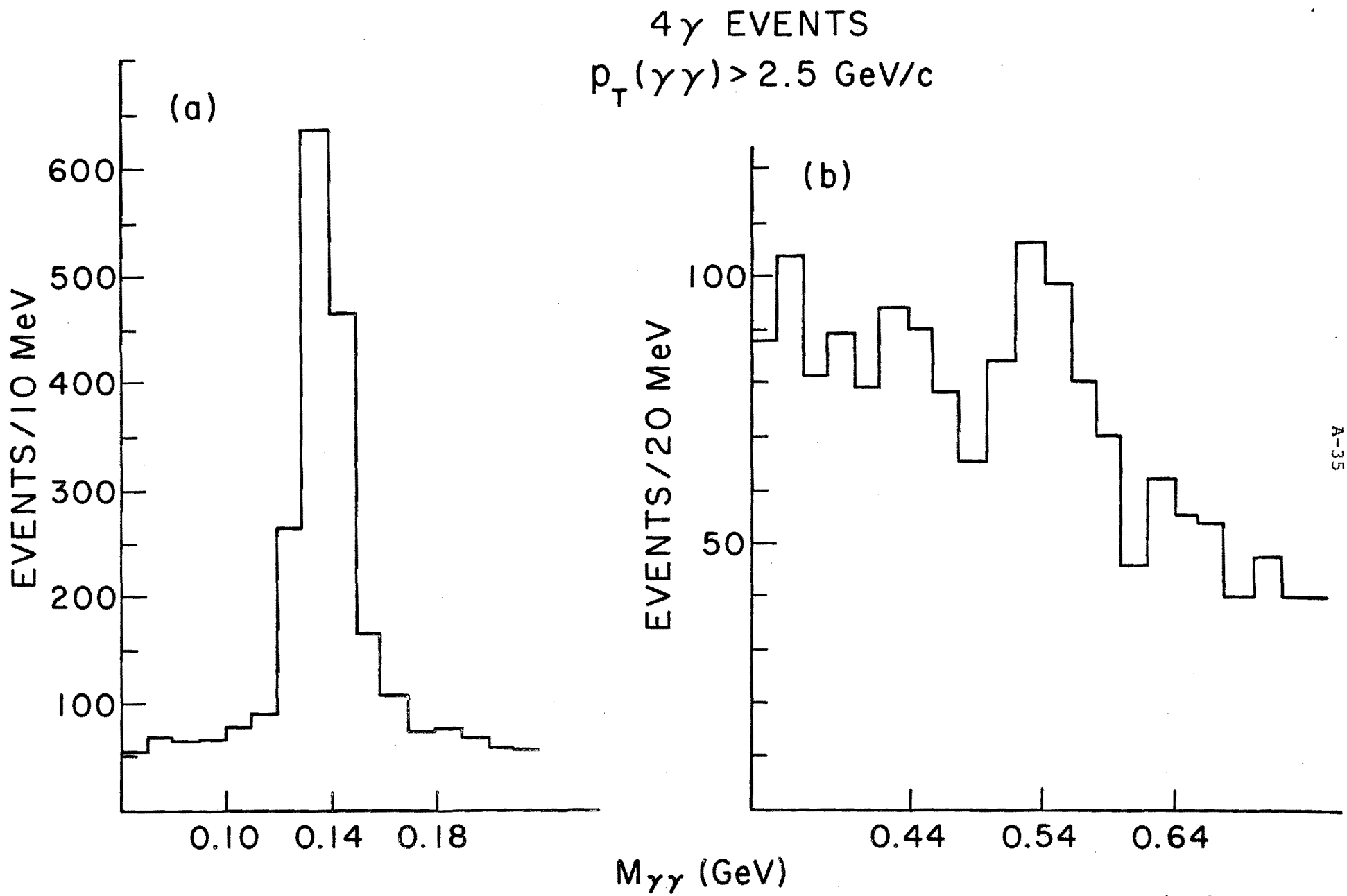
4γ EVENTS
$p_T(\gamma\gamma) > 2.5$ GeV/c
(a)
(b)
EVENTS/10 MeV
EVENTS/20 MeV
600
500
400
300
200
100
100
50
0.10
0.14
0.18
0.44
0.54
0.64
$M_{\gamma\gamma}$ (GeV)

Fig. 18

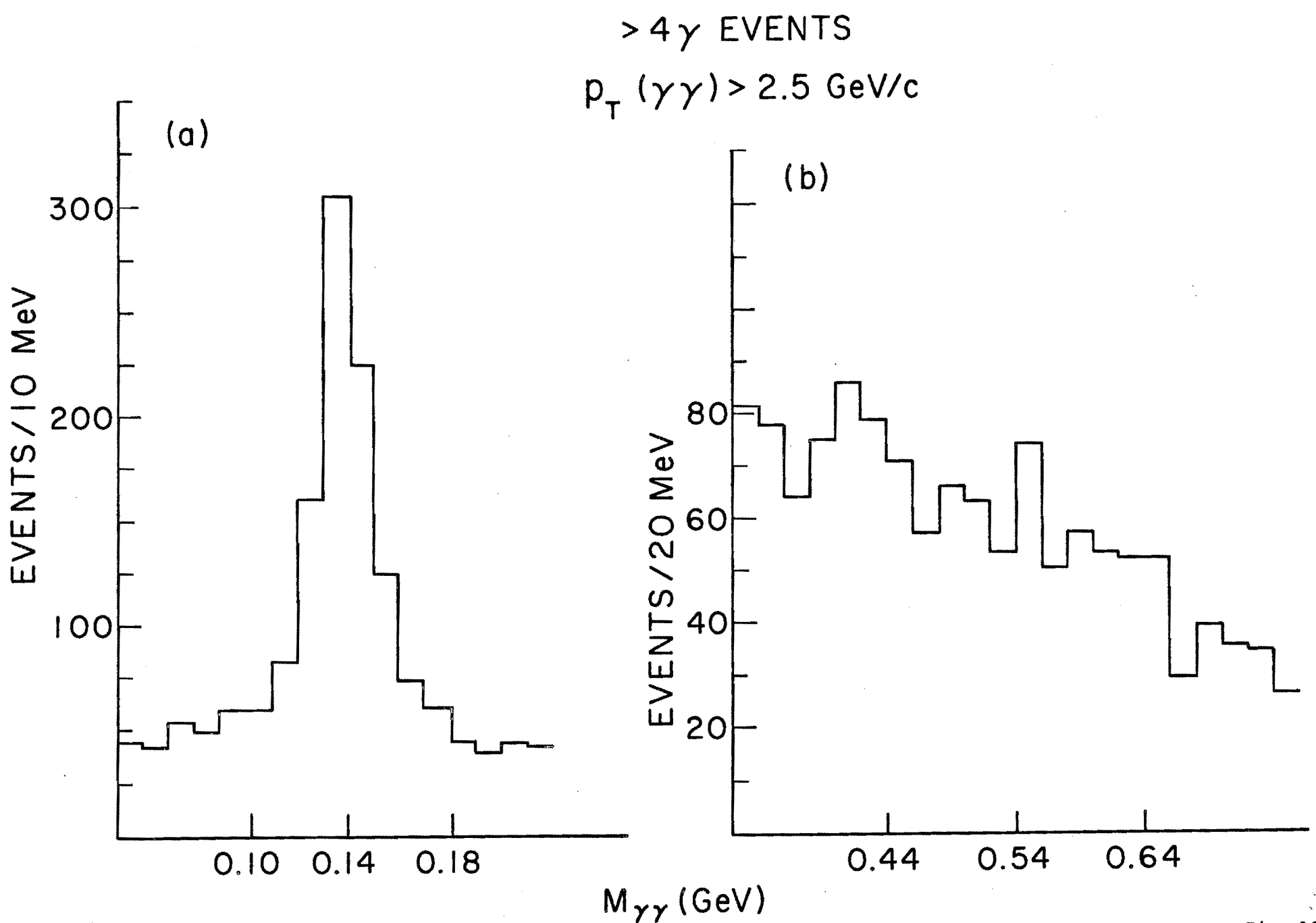
> 4γ EVENTS
p_T (γγ) > 2.5 GeV/c
(a)
(b)
EVENTS/10 MeV
EVENTS/20 MeV
300
200
100
80
60
40
20
0.10
0.14
0.18
0.44
0.54
0.64
M_γγ (GeV)

Fig. 19

APPENDIX B

The new LAC which we are proposing to build for E695 has been designed to be an optimum device for the investigation of direct photon production. It combines, in a cylindrical geometry, a calorimeter that has both electromagnetic and hadronic capability. We chose liquid argon over a gas calorimeter because we expect better stability and reliability in building a large system. Lead-scintillator calorimeters, although intrinsically faster, would be very expensive with the kind of fine segmentation we require; these types of calorimeters are also not suitable for the r-ϕ readout which we believe to be essential for the experiment. It should be noted that the crucial design parameters of the electromagnetic portion of the LAC for P695 are similar, except for the granularity, to the LAC of E272/E629; consequently we have full confidence in our ability to predict its expected performance. The parameters of our design are given in Table I of this Appendix.

(1) Resolution. Based on our actual experience using our present detector, we anticipate the following performance characteristics for the E695 LAC for photons:

(a) $\sigma_E/E \sim 14\%/\sqrt{E}$

(b) $\sigma_{space} \sim 700\ \mu$

(c) $\sigma_{time} \sim 6$ nsec

(d) $\sigma_\theta \sim 25$ mr

The basis for the first two estimates is summarized in Fig. 1, which displays data obtained in E272; the other estimates come from E629, and are based on the data displayed in Figs. 10-12 of Appendix A. The data displayed in Fig. 1 can be summarized as follows. In E272 we calibrated the LAC using a 50 GeV/c electron beam which we scanned across the detector face. The values of σ_E/E presented for the e^- calibration are the results of a channel by channel tuning of the gains and pedestals of each amplifier. It should be noted that the resolution

achieved during calibration was approximately a factor of $\sqrt{2}$ better than that obtained during actual running conditions. It is also noteworthy that the resolution obtained for a transverse scan (in which the electron beam is scanned parallel to the long dimension of the strips) is slightly but systematically worse than that obtained for an orthogonal scan (in which the electron beam is scanned perpendicularly across the long dimensions of a strip). This difference arises from pulse-height variations along a single strip, and is an example of the type of effect which leads to the overall degradation of the energy resolution in going from calibration conditions to actual running conditions. The graph of σ_E^2 vs. E was obtained from an analysis of $K^{\pm} \rightarrow e^{\pm}\pi^{o}\nu$ events acquired simultaneously with our other E272 data. The electron energies were obtained both from our drift chamber system and from the LAC, and then compared. The improvement from 1978 to 1979 arose from improvements which we made to our amplifiers and to the LAC proper during the Mesopause, which separated our two E272 data runs.

The histogram displaying the spatial resolution of the LAC was obtained by comparing the projected electron position from the drift chambers with the shower center as determined from the LAC. The fact that the spatial resolution achieved is so much narrower than the strip width itself (1.27 cm) arises because of the stability of the LAC shower shape which permitted us to derive a very accurate algorithm for determining the shower center for individual showers. The remaining histogram in Fig. 1 shows the mass resolution which we obtained during our 1979 data run. The π^{o} events originate from the reaction $\pi^{+}A \rightarrow \rho^{+}A$; $\rho^{+} \rightarrow \pi^{+}\pi^{o}$; $\pi^{o} \rightarrow \gamma\gamma$, while the η^{o} events arise from the reaction $\pi^{+}A \rightarrow A_2^{+}A$; $A_2^{+} \rightarrow \pi^{+}\eta^{o}$; $\eta^{o} \rightarrow \gamma\gamma$. We have studied the mass resolution for a two-photon system under a variety of conditions and anticipate that in E695 the bounds on that resolution will be:

$$6 \text{ MeV} \lesssim \sigma_m(\pi^{o}) \lesssim 8 \text{ MeV}$$

$$15 \text{ MeV} \lesssim \sigma_m(\eta^{o}) \lesssim 20 \text{ MeV}$$

(2) Hadron Rejection. The use of Pb plates, rather than some material of lower Z in the electromagnetic sections allows us to construct a device having a thickness of 18 radiation lengths, but only 0.9 absorption lengths in the front sections. This results in a very high level of discrimination against hadron induced showers. (For more details on this point, see Appendix A.) We wish to emphasize that a high level of hadron rejection is essential in protecting against halo-induced showers.

(3) Hadron Calorimetry. In this revised version of P695 we propose to add two hadronic calorimeter sections downstream of the electromagnetic part of the LAC. The ∿500,000 incremental cost of this addition is partially retrievable in that ∿360,000 will be used to purchase the resalable copper plates of the hadron calorimeter. The presence of a hadronic section strengthens the capability of the LAC in that it provides ability for detecting neutral hadrons and improves the resolution for charged hadrons. In addition, the use of a pad read-out in the hadronic sections will make the LAC valuable in solving pattern recognition problems for multi-photon as well as multi-charged-hadron events.

(4) New Technical Difficulties. The readout of pads (see Fig. 2) presents problems of its own. The simplest solution would be to use the two sides of each G-10 board--one side for pads and the other for the readout strips. Unfortunately, the cross capacitance between pads and readout strips for other pads would be far from negligible. The G-10 dielectric constant of $\varepsilon = 5.0$ produces a typical cross capacitance of one layer of 5-15 pF, which is to be compared with a typical capacitance to ground of 30-300 pF (depending on pad size). Thus the cross capacitance is in the range of 5-10%, tolerable if only individual pads are read out, but possibly catastrophic if the hadron layers are to be also used in the trigger. (Note that a fixed p_T implies a pulse height in the innermost pad that is about eight times the outermost one.)

We therefore propose an arrangement as shown in Figure 3. The absorber plates are alternately at H.V. and at ground. The ground plates are separated by a 1/64" insulator from a G-10 board which has the readout lines on the side towards the absorber and a solid ground plane on the other. Separated by a 2 mm LA gap is a second G-10 board which has on its away side the readout pads. The pads are connected to the readout strips by wires soldered between them. Spacers preserve the separation between the individual boards. The high voltage absorber is separated from the pads by another 2 mm LA gap. Thus there is only one readout gap per longitudinal cell--not two gaps as in the front (photon) detector.

The thickness of each absorber plate affects many other aspects of the detector, such as dewar length (see attached design note from Cryogenic Consultants), channel capacitance, resolution, cost, etc. We believe that a cell thickness of $\sim$2 cm steel equivalent is a reasonable maximum; more frequent sampling helps, especially for lower energy hadrons. A total thickness of 100 cm steel equivalent--or about seven absorption lengths--is necessary to get close to optimum resolution. However, for energies above 100 GeV a somewhat larger thickness would be preferable. In Table I we present a possible overall detector segmentation. The detector will have an overall length of $\sim$2.2 m and a total mass of $\sim$73 tons. To this has to be added $\sim$35 k liters of LA, depending somewhat on the size of the eventual cryostat.

Increasing the number of layers by finer segmentation in depth will increase the capacitance/channel. This is harmless as long as one properly compensates for it. As long as the amplifier feedback capacitance is kept proportional to the detector capacitance, the band width of the amplifier stays the same. The r.m.s. noise is then proportional to the overall channel capacitance, i.e., to the number of layers. The signal is also proportional to the sampling frequency (i.e., number of layers), and thus the signal/noise

ratio is independent of the sampling frequency. In any case, the capacitance of a single layer is quite large: for a 100 cm^2 pad it has a value of 143 pF, or with 70 layers about 10 nF. Amplification beyond the first integrating stage will therefore be required.

Table I LAC Segmentation

		Thickness	Material	Rad length	Abs length
I.	Photons	2 mm	Pb	0.357	0.011
		4 mm	LA	0.029	0.005
		1.6 mm	G-10+Cu	0.011	0.003
	Per layer	7.6 mm		0.397	0.019
	32 layers	24.3 cm		12.70	0.61
II.	Photons/Hadrons	5 mm	Cu	0.350	0.034
		4 mm	LA	0.029	0.005
		1.6 mm	G-10-Cu	0.011	0.003
	Per layer	10.6 mm		0.390	0.042
	32 layers	33.9 cm		12.48	1.34
III.	Hadrons	5 mm	Cu	0.350	0.034
		4 mm	LA	0.029	0.005
		2.8 mm	G-10+Cu	0.014	0.005
	Per layer	11.8 mm		0.393	0.044
	70 layers	82.6 mm		27.5	3.08
IV.	Hadrons	5 mm	Cu	0.350	0.034
		4 mm	LA	0.029	0.005
		2.8 mm	G-10	0.014	0.005
	Per layer	11.8 mm		0.393	0.044
	70 layers	82.6 mm		27.5	3.08
	Total Calorimeter	223.4 cm		80.2	8.11
				Weight of $\pi\times(1.6\ m)^2$	
	Total Pb	6.4 cm		5.84 tons	
	Total Cu	86.0 cm		62.0 tons	
	Total G-10	49.4 cm		7.15 tons	
	Total LA	81.6 cm		9.2 tons	
	Total Calorimeter	223.4 cm		84.2 tons	

E272/E629 LAC RESOLUTION

50 GeV/c e^- CALIBRATION

Orthogonal Scan: $\frac{\sigma_E}{E} \sim \frac{(9-10)\%}{\sqrt{E}}$

Transverse Scan: $\frac{\sigma_E}{E} \sim \frac{(11-12)\%}{\sqrt{E}}$

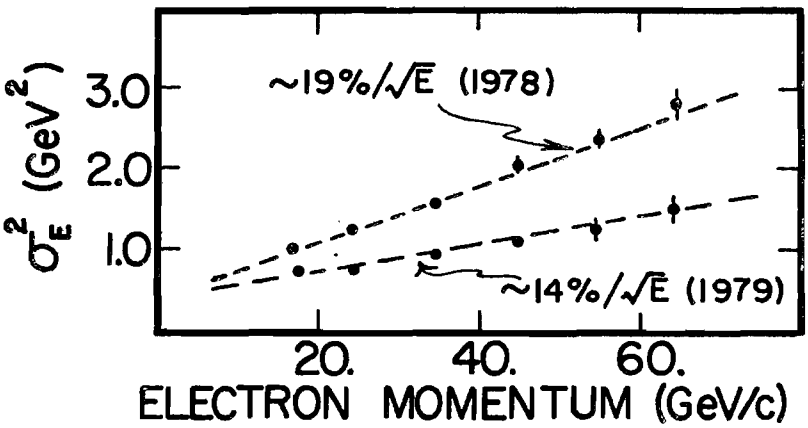

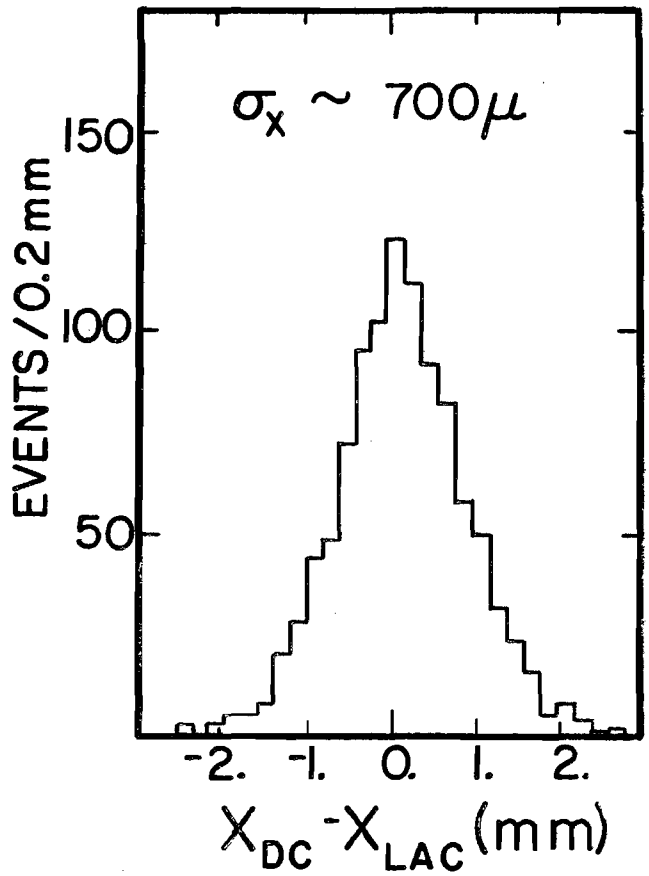

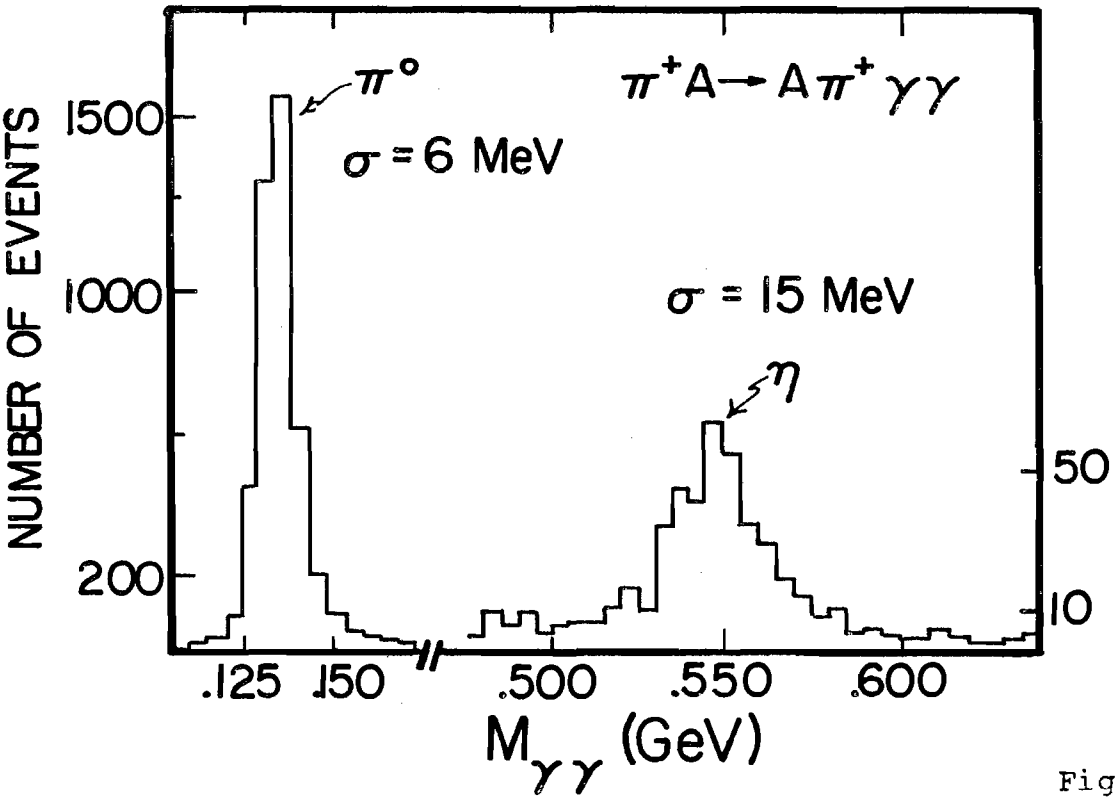

Fig. 1

TABLE OF CONTENTS

Section	Title	Page No.
1	INTRODUCTION	2
2	DESIGN	3
3	ASSEMBLY	4
4	DISCUSSION	5
5	DRAWINGS	
	5800-B - Superlad II General Arrangement	
	5801-B - Support Structure	
	5802-B - Dewar Upper Shell and Bellows Assembly	
	5803-B - Vacuum Jacket Upper Shell and Access Port	
	5804-A - Dewar End Cover	
	5805-B - Vacuum Jacket End Cover	
	5806-A - Detector	

1. INTRODUCTION:

The design, construction, and assembly regarding the construction of Superlad II have been reviewed. The physical size and limited field erection equipment combine to present a unique design challenge. This report proposes a design concept and assembly procedures to construct Superlad II with the facilities available.

In order to simplify or circumvent altogether several major problem areas, the design was based upon the following precepts:

a. Support the LAD from the bottom.

b. Accomplish elevation adjustments (if necessary) by external means.

c. Avoid the necessity of rollers within the dewar to position the detector.

d. Provide maximum access to the LAD during assembly.

e. Restrict the weight of all subassemblies to 20,000 lbs maximum (the crane capacity).

2. DESIGN:

The design concept of Superlad II is shown on the drawings attached in Section 5.

The general arrangement is shown on Dwg. No. 5800-B and consists of essentially the following subassemblies which would be field erected:

2.1 Detector support structure (Dwg. No. 5801-B) consisting of:

2.1.1 Vacuum jacket base, lower shell, and end cover.

2.1.2 Support block.

2.1.3 Dewar lower shell and end cover.

2.2 Dewar upper shell and bellows assembly (Dwg. No. 5802-B).

2.3 Vacuum jacket upper shell and access port (Dwg. No. 5803-B).

2.4 Dewar end cover (Dwg. No. 5804-A).

2.5 Vacuum jacket end cover (Dwg. No. 5805-B).

2.6 Detector (overall dimensions) (Dwg. No. 5806-A).

3. ASSEMBLY:

Superlad II would be assembled using the following assembly procedures. After each assembly milestone, the system would be integrity tested before proceding with the next phase.

3.1 The detector support structure (Dwg. No. 5801-B) shall be placed upon a suitable foundation.

3.2 The detector (Dwg. No. 5806-A) shall be assembled, segment-by-segment, upon the support structure that is integral with the lower dewar shell.

3.3 Position the dewar upper shell and bellows assembly (Dwg. No. 5802-B), and weld the shell in place.

3.4 Position the vacuum jacket upper shell and access port (Dwg. No. 5803-B), and weld the shell. Weld the bellows assembly to the inside of the access port.

3.5 Attach instrumentation from detector through access port, and check thoroughly.

3.6 Weld dewar end cover (Dwg. No. 5804-A) in place. Check dewar for integrity.

3.7 Weld vacuum jacket end cover (Dwg. No. 5805-B) in place. Check vacuum jacket for integrity.

4. DISCUSSION:

4.1 Support Structure:

The weight of the internal detector is estimated to be approximately 60 tons. Combined with the inner vessel and LA, the total weight is expected to be on the order of 80-100 tons.

Although at first glance, it would appear that this is not too great a weight to suspend from a 1/8 in. thick 2M diameter shell, the structure required to transmit the load to a rigid foundation becomes complicated. Therefore, it was decided to support the detector from the bottom.

The detector base would be mounted to framework within the dewar. Phenolic blocks (G-10) would be positioned between the dewar and the vacuum jacket. A rigid base and cradle would be permanently attached to the vacuum jacket.

Assuming 100 tons (2×10^5 lbs) maximum is transmitted through the phenolic blocks, the required bearing area would be:

$$A = \frac{2 \times 10^5 \text{ lbs}}{5000 \text{ psi}} = 40 \text{ in.}^2$$

This is a relatively small area and can quite easily be fitted into the annular space between the dewar and the vacuum jacket.

4.2 Elevation Adjustments:

Elevation adjustments can quite easily be incorporated into the vacuum jacket base. Either mechanized or manually operated leveling/adjusting screws can be secured to the foundation and act upon the base to move it into the desired location.

4.3 Elimination of Internal Rollers:

Because all rollers capable of supporting heavy machinery use some sort of grease which presents the danger of contaminating the LA, it was decided to eliminate the need for rollers within the dewar.

By constructing the dewar in segments and, in effect, build the detector upon the lower half of the dewar and vacuum jacket, the entire upper portion is directly acccessible from the top. Detector segments could be positioned by crane. Roller alignment to access tracks, cantilevered structures, or removal of rollers after each segment is positioned is thereby eliminated.

4.4 Maximum Accessibility:

Another advantage gained from assembling the detector upon the lower half of the dewar is good accessibility. The detector would be accessible from three sides and from a large portion of the fourth side as well as from the top.

Such accessibility would relax design restrictions on the detector and could manifest itself in lower costs.

4.5 Weight Restrictions:

All subassemblies would be restricted to a weight of 20,000 lbs maximum to comply with the crane limitation.

The design concept proposed allows each component to be positioned directly from above. Even at full allowable weight, positioning of components by this method is easier than cantilevering or rolling components half their weight into position.

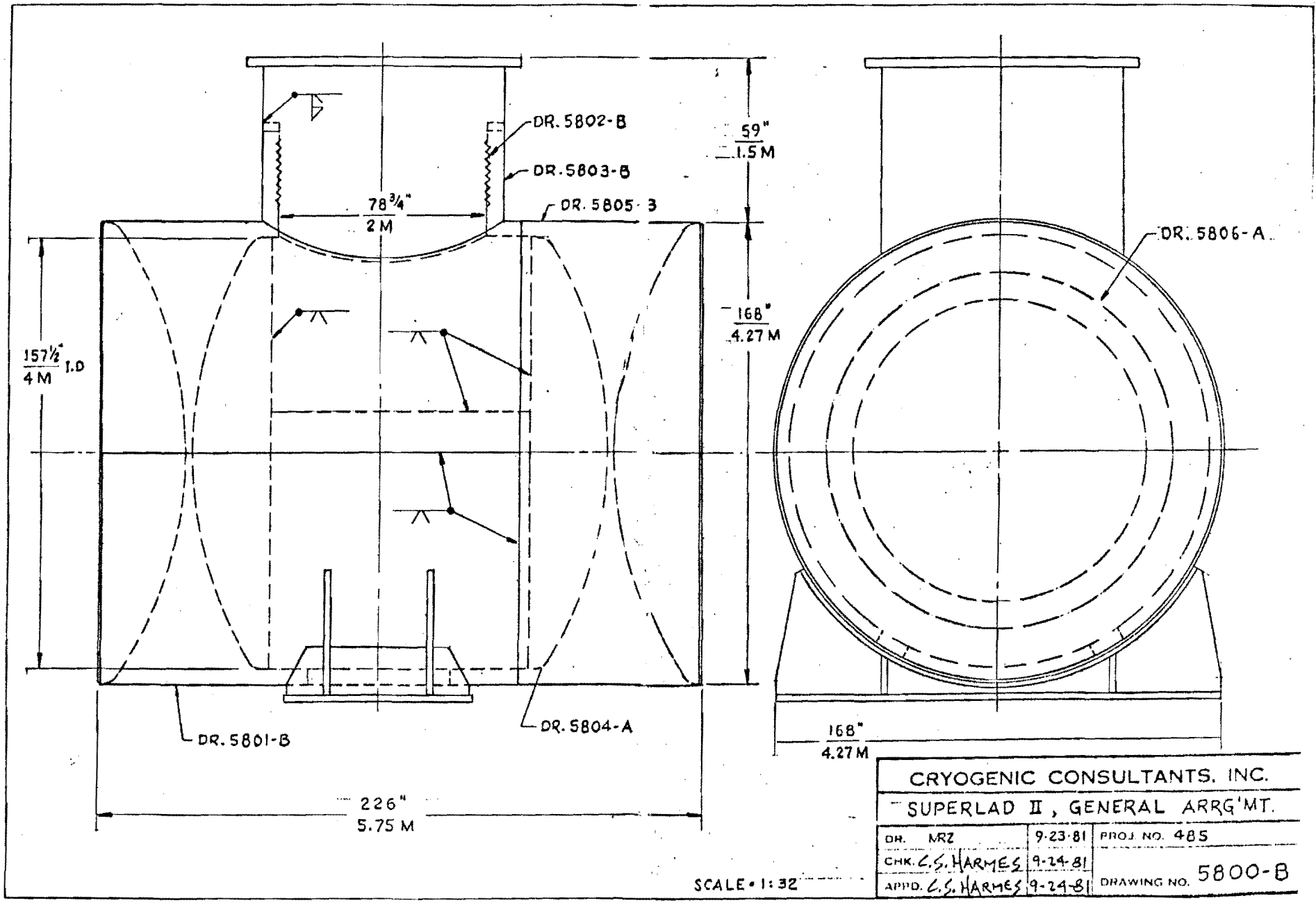
DR. 5802-B
DR. 5803-B
DR. 5805-B
DR. 5806-A
DR. 5801-B
DR. 5804-A
78 3/4"
2 M
59"
1.5 M
168"
4.27 M
157 1/2"
4 M
I.D
226"
5.75 M
168"
4.27 M
SCALE = 1:32
CRYOGENIC CONSULTANTS, INC.
SUPERLAD II, GENERAL ARRG'MT.
DR. MRZ
9-23-81
PROJ. NO. 485
CHK. C.S. HARMES
9-24-81
APPD. C.S. HARMES
9-24-81
DRAWING NO. 5800-B

APPENDIX C

Since the liquid argon photon/hadron calorimeter has a sizeable hole surrounding the beam region, a conventional calorimeter, capable of high-rate operation, has been designed to cover almost all of the forward region. This calorimeter extends the region capable of jet definition into very small angles (3 mr), sharpens the total energy definition and allows us to study the fragmentation of the incident hadron. The specific aims are good total energy resolution and good resolution in transverse momentum, for multi-particle forward events.

In forward multi-hadron events, with a typical set of calorimeter responses ($\Delta E = K\sqrt{E}$, $K \lesssim 100\%$; $\Delta\Theta$ fixed, by module size) the transverse momentum resolution is dominated by $\Delta\Theta$. (The parameter K controls the energy resolution). Thus the resolution is given (roughly) by $\Delta p_t = p_{mx} \Delta\Theta$ where p_{mx} is the laboratory momentum of the highest energy particle in the forward jet. A typical value might be $p_{mx} = 250$ GeV/c; thus an angular resolution of 2 mr will insure that $\Delta p_t \lesssim 0.5$ GeV/c.

The design presented here consists of a stack of 108 modules, each with a cross-section of $2\frac{1}{2}''\times 2\frac{1}{2}''$, $(6.35\ \text{cm})^2$. This leads to a σ of 1.4 mr in each transverse coordinate, or 2 mr in the full angle. Each module consists of alternate layers of 19mm Fe and acrylic scintillator, totalling 8.0 absorption lengths. The acrylic is sampled by a triangular-cross-section BBQ bar which constitutes a corner of the square cross-section. A sketch of the stack is shown in Figure C-1 (where the overlap with the LAC is also indicated) and a schematic of a module is shown in Figure C-2.

A design very similar to the one presented here has been described by Yost et al. (IEEE, Vol. NS-26, 1979). The response of that design was found to be $\Delta E = 0.8\sqrt{E}$, well within our requirements. The modules will be subdivided longitudinally into two 1-meter segments,

with four absorption lengths each. This provides a two-fold benefit: the attenuation in the BBQ read-out bars is reduced considerably; and the small (2%) "cold" spot introduced by the lack of iron in the read-out channel can be partially mitigated by rotating the back set of modules 180° about the beam axis. These cold spots are small in any case: their angular "acceptance" is comparable with the minimum accepted by the calorimeter, thus any particle that originates in the target has a small probability of traversing only the BBQ. The same considerations apply even more strongly to particles that try to slip in between modules.

The angular coverage of the calorimeter (situated 13 meters from the target) is from 3.5 mr to 27 mr, total, and from 2.5 mr to 27 mr in the horizontal and vertical projections. It corresponds, roughly, to a circle of 70 cm diameter with one $(6.35\ \text{cm})^2$ hole, representing one absent module, for the passage of the non-interacting beam particles. The phototubes connected to the BBQ bars are connected to fast ADC's, but this information is not utilized in trigger formation.

TABLE C-1 Calorimeter Characteristics

Energy Resolution	$\Delta E/E = 0.8/\sqrt{E(\text{GeV})}$
Angular Resolution	$\Delta\theta = 2\times10^{-3}$ radians
p_t Resolution	$\Delta p_t \approx 0.5$ GeV/c, typical
Segmentation	64x(19mm Fe, 12mm acrylic)
Length	2.01 meters, 8.0 absorption lengths
Module count	2x(108 modules) ; 2x(1-meter lengths)

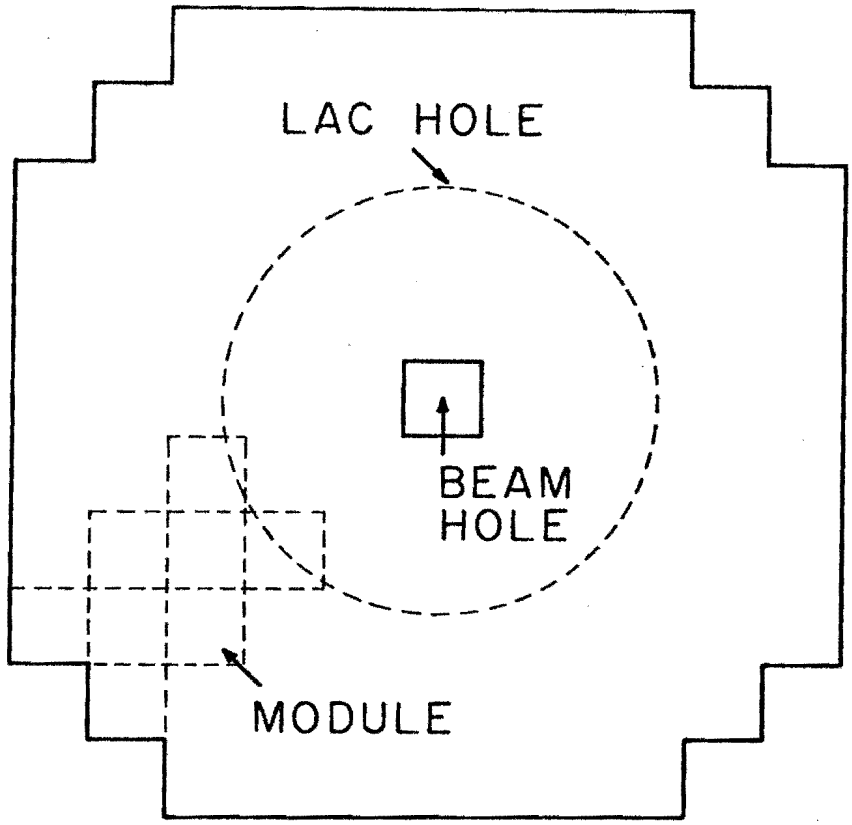

Figure C.1 THE CALORIMETER STACK

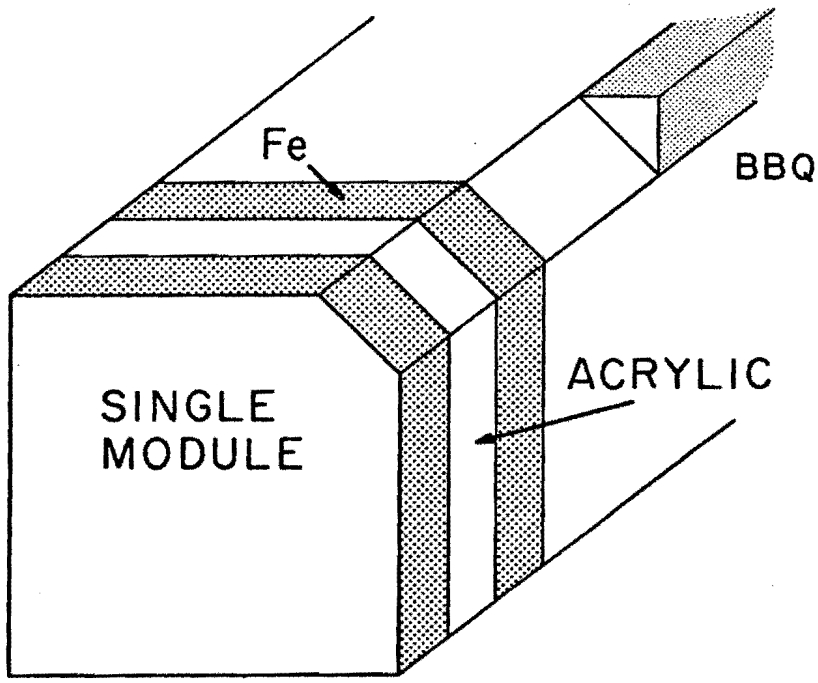

Figure C.2 CALORIMETER MODULE

APPENDIX D

We give an estimate of the expected costs to construct the equipment for E695. The individual component costs of each subsystem are identified as far as possible. We include machining and technician costs; the physicist manpower is not included. We also do not include any overhead costs, because they differ between institutions. Finally, no contingency amounts are included and escallation of costs by delays and inflation is ignored. We have also not included the costs of magnets, floor modification, shielding, rigging, etc., nor the costs of the computer to perform the on-line readout and checks. We have tried to be conservative in our cost estimates, but must warn that they have to be considered preliminary pending further detailed engineering studies.

The overall equipment cost of about 2.6M$ is quite moderate considering the scope of the experiment.

			Total (in thousands)
Table D.1. LIQUID ARGON PHOTON/HADRON DETECTOR			
I. Main Detector			
G-10 boards	$ 90		
Lead sheets	80		
Copper plates	350		
Cradle	70		
Spacers	50		
Connectors	40	$ 680	
II. Cryogenics			
Detector dewar	270		
Storage dewar	50		
Transfer lines, thermometry, pumps, ...	40		
Initial LA fill	60	420	
III. Electrical Components			
Mylar cables and feedthroughs	40		
Capacitors	90		
Amplifiers	350		
Local and global p_T trigger	40		
TDC's	60		
Cables	30		
Noise suppression equipment	40	650	$1750
Table D.2. PROPORTIONAL CHAMBER SYSTEM			
Frames and stands	100		
Amplifiers for 12,500 wires	315		
Cabling	10		425
Table D.3 SOLID STATE DETECTORS			
Amplifiers for 3000 wires	150		
Detectors (7 layers)	10		
Mounting and alignment fixtures	20		180
Table D.4 FORWARD CALORIMETER			
216 channels (PM and amplifiers)	30		
Steel	40		
Acrylic	30		
Assembly and supports	30		130
Table D.5. MISCELLANEOUS			
Transition counters	50		
Target stands	10		
Peripheral microcomputers (3)	30		
Long distance cabling	10		100
TOTAL			$2585